Received: 3 August 2021 | Revised: 27 April 2022 | Accepted: 12 July 2022

IET Quantum Communication

DOI: 10.1049/qtc2.12048

The Institution of Engineering and Technology WILEY

ORIGINAL RESEARCH

Complexity analysis of quantum teleportation via different entangled channels in the presence of noise

Deepak Singh[1] | **Sanjeev Kumar**[1,2] | **Bikash K. Behera**[3]

[1]Department of Mathematics, Indian Institute of Technology Roorkee, Roorkee, Uttarakhand, India

[2]Mehta Family School of Data Science and Artificial Intelligence, Indian Institute of Technology Roorkee, Roorkee, Uttarakhand, India

[3]Bikash's Quantum (OPC) Pvt. Ltd, Nadia, West Bengal, India

Correspondence

Deepak Singh, Department of Mathematics, Indian Institute of Technology, Roorkee 247667, Uttarakhand, India.
Email: dsingh@ma.iitr.ac.in

Funding information

Science and Engineering Research Board, Grant/Award Number: SERB/2020/002040

Abstract

Quantum communication is an integral part of quantum computing, where teleportation of a quantum state has gained significant attention from researchers. Many teleportation schemes have been introduced in the recent past. In this study, the authors compare the teleportation of a single-qubit message among different entangled channels such as the two-qubit Bell channel, three-qubit GHZ channel, two/three-qubit cluster states, a highly entangled five-qubit state (Brown et al.) and the six-qubit state (Borras et al.). The authors calculate and compare the quantum costs for these channels. The authors also study the effects of six noise models: bit-flip noise, phase-flip noise, bit-phase-flip noise, amplitude damping, phase damping and depolarising error. These noise models may affect the communication channel used for teleportation. An investigation of the variation of the initial state's fidelity is performed for the teleported state in the presence of the noise model. It is observed that the fidelity decreases in all the entangled channels as the noise parameter η increases in the range [0, 0.5] for all the noise models. The fidelity shows an upward trend in the Bell, GHZ and three-qubit cluster state channels, as η varies in the range [0.5, 1.0] for all the noise models. However, in the rest of the three channels, the fidelity substantially decreases in the case of amplitude damping, phase damping and depolarising noise, and even it reaches zero for $\eta = 1$ in Brown et al. and Borras et al. channels.

1 | INTRODUCTION

Quantum communication deals with the transmission of the quantum states between distance sites. It plays a prominent role in quantum information processing [1, 2]. Quantum communication is improving day by day with the improvement in current technological advancement. Quantum networking has a broad spectrum of applications, quantum devices such as quantum routers [3–6], quantum repeaters [7–11], quantum satellite have been developed recently by China [12–14], which claims itself to be secure. Security is an essential aspect of today's communication. When we have cloud data storage, there is always a threat of breaking into the data in the present era. Many quantum communication protocols have been developed such as quantum cryptography [15–17], quantum information sharing [18–21], quantum superdense coding [22, 23], quantum remote state preparation [24, 25], quantum hierarchical remote state preparation [26, 27], and quantum teleportation [28–31] to name a few.

Quantum teleportation transmits quantum information from one place to another via a shared entangled channel, which can be obtained by measurement in classical physics. Entanglement plays a key role in quantum teleportation because of its non-local properties. When an entangled quantum state is shared between two or more parties, they can teleport a message using the entangled channel. They must apply certain unitary operations on appropriate qubits to teleport the message to a particular qubit. The first time quantum teleportation was proposed by Bennett et al. [28] in 1993 via Einstein–Podolsky–Rosen (EPR). After that, many different protocols are put forward with the extension of qubits [32] and dense coding [33]. Quantum teleportation is implemented experimentally in some of the research studies presented [29–31, 34] in various quantum systems. Apart from

that, many theoretical and experimental quantum teleportation schemes have been proposed by researchers so far [35–41]. In Ref. [42], two different schemes were proposed for teleporting a single-qubit state by using the W state. In Ref. [43] a generalised teleportation scheme of an entangled state was proposed using a Greenberger–Horne–Zeilinger (GHZ)-class state. Several new schemes are proposed for teleportation using the W state and the GHZ state or the GHZ-like state [44]. The cluster states channel is used in Ref. [45] to teleport arbitrary two states using a four-qubit cluster state. The teleportation of a three-qubit state using the five-qubit cluster state is also performed in Ref. [46]. Then quantum teleportation of an arbitrary two-qubit state has been performed using a four-qubit cluster state [47]. Quantum controlled teleportation of random qubit states has also been demonstrated via cluster states [48]. Then, some new schemes of quantum teleportation were proposed using entanglement in coined quantum walk [49–51], which has attracted the tremendous attention of the scientific community. In Ref. [52], the fidelity of quantum teleportation under noisy channels are studied. An experimental study of the teleportation under the effect of noise can be found in Ref. [53]. Also, quantum teleportation in higher dimensions under the effect of noise is studied in Ref. [54]. They demonstrated that all conceivable circumstances can be divided into four different behaviours and discussed cases where increasing the corresponding noise percentages could increase fidelity.

In this study, we have performed a complexity analysis of the teleportation of a single-qubit message using different entangled channels such as the Bell channel, three-qubit GHZ channel, two-qubit cluster state, three-qubit cluster state, highly entangled five-qubit Brown et al. state and the six-qubit Borras et al. state. Here, we apply quantum gates on the circuit to perform the teleportation. As the number of quantum gates increases in a protocol, it increases the complexity of teleportation. Therefore, we have calculated the quantum cost for all the above teleportation protocols and a graphical histogram representation is made in Figure 9 to compare the quantum cost of different teleportation protocols. Any actual quantum experiment cannot be performed without noise in the channel. Noise is an inevitable feature of quantum communication that affects teleportation. The noise in the quantum system changes its state from a pure state to a mixed state; therefore, some quantum information is lost during teleportation. Hence, we have introduced some noisy environments into each entangled channel used for teleportation. We have taken the six types of noise that may affect the teleportation process: bit-flip noise, phase-flip noise, bit-phase-flip noise, amplitude damping, phase damping and depolarising noise. We have analytically derived the density matrices for all the entangled channels under every noise model. As fidelity gives the closeness between the two quantum states, we have calculated the fidelity between the initial and teleported states under noise. Then, a visual representation is made by plotting a graph between the noise parameter and the fidelity.

The rest of the paper is organised as follows: Section 2 contains some basic definitions and the teleportation processes. In Section 3, the analysis of noise in the entangled channel used for teleportation is presented. Finally, we conclude in Section 4 with some discussion about findings followed by the future directions.

2 | PRELIMINARIES

2.1 | Quantum cost

Quantum cost is the number of primitive reversible gates used in designing a circuit. The quantum cost of all basic single-qubit gates and control not is taken as unity [55]. One [55] of the essential properties of each reversible gate is that it can be generated from a combination of basic quantum gates. Therefore, the quantum cost of each reversible gate can be calculated by counting the number of related basic gates. The Hadamard and control-not (CNOT) gates have a quantum cost equal to one. The other gates used in this paper are the control-Z gate and SWAP gates. These gates can be implemented with the help of Hadamard and CNOT gates as shown in Figures 1 and 2, respectively. The more the quantum cost, the more complexity will be in executing the circuit on the actual quantum hardware. So in the next section, we have evaluated the quantum cost of each teleportation protocol via different entangled channels.

2.2 | Teleportation schemes

2.2.1 | Teleportation using Bell channel

An arbitrary single-qubit quantum message can be written as $|M\rangle = \alpha|0\rangle + \beta|1\rangle$, where $\alpha, \beta \in \mathbb{C}$ and $|\alpha|^2 + |\beta|^2 = 1$. A more convenient representation of the single-qubit state is given by the following expression $|M\rangle = \cos(\theta/2)|0\rangle + e^{i\phi}\sin(\theta/2)|1\rangle$, where $\theta \in [0, \pi]$ and $\phi \in [0, 2\pi]$. The teleportation of this single-qubit message is carried out using the two-qubit Bell channel given by $|\psi^{\pm}\rangle = \frac{1}{\sqrt{2}}(|00\rangle \pm |11\rangle)$, $|\phi^{\pm}\rangle = \frac{1}{\sqrt{2}}(|01\rangle \pm |10\rangle)$. The entangled Bell channel is shared between two parties, say Alice and Bob. Alice has the first qubit and Bob has the second qubit that form the entangled Bell channel. Now, choose one of the Bell channels for teleportation process, say $|\psi^{+}\rangle$; the combined state after taking the

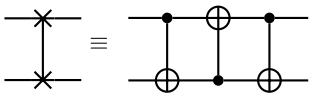

FIGURE 1 SWAP gate decomposition

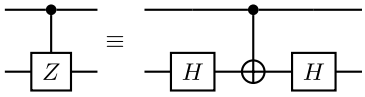

FIGURE 2 Control-Z gate decomposition

tensor product of $|M\rangle$ and $|\psi^+\rangle$ is given in Equation (1). Now, Alice applies the Bell basis measurement on the first and second qubit, that is $CX(1, 2)$ (Qubit 1 is control qubit and qubit 2 is target qubit) and $H(1)$ (Hadamard gate on qubit 1), and the final state $|\xi_f\rangle$ is shown in Equation (2),

$$\begin{aligned}|\xi\rangle &= |M\rangle_1 \otimes |\psi^+\rangle_{23} \\ &= (\alpha|0\rangle + \beta|1\rangle)_1 \otimes \left(\frac{1}{\sqrt{2}}(|00\rangle + |11\rangle)_{23}\right)\end{aligned} \tag{1}$$

$$\begin{aligned}|\xi_f\rangle = &\frac{|00\rangle_{12}}{2}(\alpha|0\rangle + \beta|1\rangle)_3 + \frac{|01\rangle_{12}}{2}(\alpha|1\rangle + \beta|0\rangle)_3 \\ &+ \frac{|10\rangle_{12}}{2}(\alpha|0\rangle - \beta|1\rangle)_3 + \frac{|11\rangle_{12}}{2}(\alpha|1\rangle - \beta|0\rangle)_3\end{aligned} \tag{2}$$

The teleportation of the single-qubit message $|M\rangle$ at this stage has been achieved successfully to Bob's qubit. However, now Bob needs to apply appropriate unitary operations on his qubit to recover the teleported message. The teleportation protocol is prepared via the quantum circuit given in Figure 3. The controlled operations are represented in the circuit 3 after the red dash line. Here in the quantum circuit, $|a\rangle, |b\rangle \in \{|0\rangle, |1\rangle\}$. Choosing different values of $|a\rangle$ and $|b\rangle$ we get different Bell channels as shown in Table 1.

Alice uses a classical channel to convey her measurement result to Bob after she has conducted the Bell basis measurement on the first two qubits. To recover the message and complete the teleportation process, Bob uses the proper unitary operation on his qubit shown in Table 2. The controlled operations in the case of the Bell channel $|\psi_+\rangle = \frac{1}{\sqrt{2}}(|00\rangle + |11\rangle)$ are given in the quantum circuit (Figure 3) after the red dashed line.

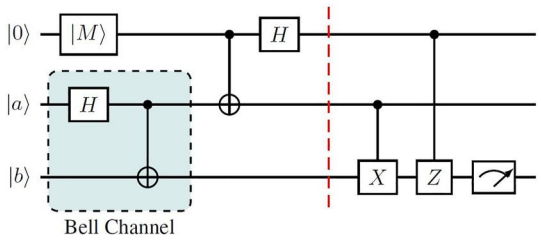

FIGURE 3 Quantum circuit for teleporting the message $|M\rangle$ through the Bell channels; controlled operations are represented for $|\psi_1\rangle$ (given in Table 1) after the red dashed line

TABLE 1 All possible Bell channels, choosing different values of $|a\rangle$ and $|b\rangle$

$\|a\rangle$	$\|b\rangle$	Bell states	Quantum cost
$\|0\rangle$	$\|0\rangle$	$\|\psi^+\rangle = \frac{1}{\sqrt{2}}(\|00\rangle + \|11\rangle)$	9
$\|0\rangle$	$\|1\rangle$	$\|\phi^+\rangle = \frac{1}{\sqrt{2}}(\|01\rangle + \|10\rangle)$	11
$\|1\rangle$	$\|0\rangle$	$\|\psi^-\rangle = \frac{1}{\sqrt{2}}(\|00\rangle - \|11\rangle)$	11
$\|1\rangle$	$\|1\rangle$	$\|\phi^-\rangle = \frac{1}{\sqrt{2}}(\|01\rangle - \|10\rangle)$	13

Note: The last column contains the quantum cost for teleporting single-qubit message via different Bell channels.

2.2.2 | Teleportation using GHZ channel

Consider the three-qubit GHZ channel as the underlying entangled channel for teleportation. The quantum state of the three-qubit GHZ channel is defined as $|\psi_i\rangle = \frac{1}{\sqrt{2}}(|x_1x_2x_3\rangle \pm |\bar{x}_1\bar{x}_2\bar{x}_3\rangle)_{123}$, where $x_1, x_2, x_3 \in \{0, 1\}$ and $\bar{x}_1, \bar{x}_2, \bar{x}_3$ are their respective conjugates. Here, the first qubit belongs to Alice, second qubit belongs to a controller Charlie and third qubit belongs to Bob. To teleport the message $|M\rangle = \alpha|0\rangle + \beta|1\rangle$ through one of the GHZ channels, say $|\psi_1\rangle = \frac{1}{\sqrt{2}}(|000\rangle + |111\rangle)_{123}$, the tensor product of $|M\rangle$ and $|\psi_1\rangle$ is taken. Then Alice applies the Bell basis measurement on the first and second qubit, that is, $CX(1, 2)$ and $H(1)$, Charlie applies Hadamard gate on the third qubit $H(3)$, and the final state is shown by Equation (3).

TABLE 2 Controlled operations that Bob needs to apply to recover the teleported message $|M\rangle = \alpha|0\rangle + \beta|1\rangle$ via all four Bell channels

	Control operations for different Bell channels			
Alice's measurement	$\|\psi^+\rangle$	$\|\psi^-\rangle$	$\|\phi^+\rangle$	$\|\phi^-\rangle$
$\|00\rangle$	$\mathbb{I}$	$\mathbb{Z}$	$\mathbb{X}$	$\mathbb{ZX}$
$\|01\rangle$	$\mathbb{X}$	$\mathbb{ZX}$	$\mathbb{I}$	$\mathbb{Z}$
$\|10\rangle$	$\mathbb{Z}$	$\mathbb{I}$	$\mathbb{ZX}$	$\mathbb{X}$
$\|11\rangle$	$\mathbb{ZX}$	$\mathbb{X}$	$\mathbb{Z}$	$\mathbb{I}$

TABLE 3 Three-qubit GHZ states after choosing different combinations of $|a\rangle$, $|b\rangle$ and $|c\rangle$

$\|a\rangle$	$\|b\rangle$	$\|c\rangle$	GHZ state	Quantum cost
$\|0\rangle$	$\|0\rangle$	$\|0\rangle$	$\|\psi_1\rangle = \frac{1}{\sqrt{2}}(\|000\rangle + \|111\rangle)$	12
$\|0\rangle$	$\|0\rangle$	$\|1\rangle$	$\|\psi_2\rangle = \frac{1}{\sqrt{2}}(\|001\rangle + \|110\rangle)$	13
$\|0\rangle$	$\|1\rangle$	$\|0\rangle$	$\|\psi_3\rangle = \frac{1}{\sqrt{2}}(\|010\rangle + \|101\rangle)$	13
$\|0\rangle$	$\|1\rangle$	$\|1\rangle$	$\|\psi_4\rangle = \frac{1}{\sqrt{2}}(\|000\rangle - \|111\rangle)$	14
$\|1\rangle$	$\|0\rangle$	$\|0\rangle$	$\|\psi_5\rangle = \frac{1}{\sqrt{2}}(\|011\rangle + \|100\rangle)$	15
$\|1\rangle$	$\|0\rangle$	$\|1\rangle$	$\|\psi_6\rangle = \frac{1}{\sqrt{2}}(\|001\rangle - \|110\rangle)$	18
$\|1\rangle$	$\|1\rangle$	$\|0\rangle$	$\|\psi_7\rangle = \frac{1}{\sqrt{2}}(\|010\rangle - \|101\rangle)$	15
$\|1\rangle$	$\|1\rangle$	$\|1\rangle$	$\|\psi_8\rangle = \frac{1}{\sqrt{2}}(\|011\rangle - \|100\rangle)$	20

Note: The last column contains the quantum cost for teleporting a single-qubit message via the GHZ states.

Abbreviation: GHZ, Greenberger–Horne–Zeilinger.

TABLE 4 Controlled operations that Bob needs to apply to recover the teleported message $|M\rangle = \alpha|0\rangle + \beta|1\rangle$ via all the eight possible GHZ channels

Alice's measurement (Qubit{1,2})	Charlie's measurement Qubit{3}	Bob's operation (Qubit{4})							
		$\|\psi_1\rangle$	$\|\psi_2\rangle$	$\|\psi_3\rangle$	$\|\psi_4\rangle$	$\|\psi_5\rangle$	$\|\psi_6\rangle$	$\|\psi_7\rangle$	$\|\psi_8\rangle$
$\|00\rangle$	$\|0\rangle$	$\mathbb{I}$	$\mathbb{Z}$	$\mathbb{X}$	$\mathbb{ZX}$	$\mathbb{I}$	$\mathbb{Z}$	$\mathbb{X}$	$\mathbb{ZX}$
	$\|1\rangle$	$\mathbb{Z}$	$\mathbb{I}$	$\mathbb{ZX}$	$\mathbb{X}$	$\mathbb{Z}$	$\mathbb{I}$	$\mathbb{ZX}$	$\mathbb{X}$
$\|01\rangle$	$\|0\rangle$	$\mathbb{X}$	$\mathbb{ZX}$	$\mathbb{I}$	$\mathbb{Z}$	$\mathbb{X}$	$\mathbb{ZX}$	$\mathbb{I}$	$\mathbb{Z}$
	$\|1\rangle$	$\mathbb{ZX}$	$\mathbb{X}$	$\mathbb{Z}$	$\mathbb{I}$	$\mathbb{ZX}$	$\mathbb{X}$	$\mathbb{Z}$	$\mathbb{I}$
$\|10\rangle$	$\|0\rangle$	$\mathbb{Z}$	$\mathbb{I}$	$\mathbb{ZX}$	$\mathbb{X}$	$\mathbb{Z}$	$\mathbb{I}$	$\mathbb{ZX}$	$\mathbb{ZX}$
	$\|1\rangle$	$\mathbb{I}$	$\mathbb{Z}$	$\mathbb{X}$	$\mathbb{ZX}$	$\mathbb{I}$	$\mathbb{Z}$	$\mathbb{X}$	$\mathbb{X}$
$\|11\rangle$	$\|0\rangle$	$\mathbb{ZX}$	$\mathbb{X}$	$\mathbb{Z}$	$\mathbb{Z}$	$\mathbb{ZX}$	$\mathbb{X}$	$\mathbb{Z}$	$\mathbb{I}$
	$\|1\rangle$	$\mathbb{X}$	$\mathbb{ZX}$	$\mathbb{I}$	$\mathbb{I}$	$\mathbb{X}$	$\mathbb{ZX}$	$\mathbb{I}$	$\mathbb{Z}$

Abbreviation: GHZ, Greenberger–Horne–Zeilinger.

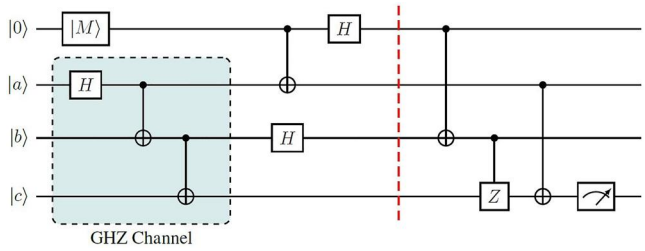

FIGURE 4 Teleportation protocol of a single-qubit message $|M\rangle = \alpha|0\rangle + \beta|1\rangle$ using entangled GHZ channel; controlled operations are represented for $|\psi_1\rangle$ (given in Table 3) after the red dashed line, which will vary for different GHZ channels. GHZ, Greenberger–Horne–Zeilinger

$$
\begin{aligned}
|\xi\rangle &= |M\rangle_1 \otimes |\psi_1\rangle_{234} \\
&= \frac{|00\rangle_{12}}{2}\left(|0\rangle_3(\alpha|0\rangle + \beta|1\rangle)_4 + |1\rangle_3(\alpha|0\rangle - \beta|1\rangle)_4\right) \\
&\quad + \frac{|01\rangle_{12}}{4}\left(|0\rangle_3(\alpha|1\rangle + \beta|0\rangle)_4 + |1\rangle_3(-\alpha|1\rangle + \beta|0\rangle)_4\right) \\
&\quad + \frac{|10\rangle_{12}}{4}\left(|0\rangle_3(\alpha|0\rangle - \beta|1\rangle)_4 + |1\rangle_3(\alpha|0\rangle + \beta|1\rangle)_4\right) \\
&\quad + \frac{|11\rangle_{12}}{4}\left(|0\rangle_3(\alpha|1\rangle - \beta|0\rangle)_4 + |1\rangle_3(-\alpha|1\rangle - \beta|0\rangle)_4\right)
\end{aligned} \tag{3}
$$

Here, the single-qubit message $|M\rangle = \alpha|0\rangle + \beta|1\rangle$ has been teleported to Bob's qubit successfully. Before making a measurement, Bob needs to apply proper unitary operations on his qubit to recover the message. The unitary operations are shown in Table 4. The teleportation protocol via GHZ channel is demonstrated via the following quantum circuit (Figure 4), where $|a\rangle, |b\rangle, |c\rangle \in \{|0\rangle, |1\rangle\}$, choosing different combinations of values of $|a\rangle, |b\rangle$ and $|c\rangle$; all of the eight three-qubit GHZ states are shown in Table 3. To recover the teleported messages, Bob needs to apply certain controlled unitary operations to his qubit. For all of the eight entangled GHZ channels, the controlled operations are given in Table 4.

2.2.3 | Teleportation using two-qubit cluster state channel

The two-qubit cluster state is an entangled channel shared by the parties Alice and Bob to perform the teleportation. It is given by $|\psi_i\rangle = (|a\rangle|b\rangle)_{CZ(1,2)}$, where $|a\rangle, |b\rangle \in \{|+\rangle, |-\rangle\}$. The two-qubit cluster state channel is prepared inside the dashed box in the circuit given in Figure 5. Taking $|a\rangle = |+\rangle$ and $|b\rangle = |+\rangle$, the two-qubit cluster state is given by, $|\psi_1\rangle = (|+\rangle|+\rangle)_{CZ(1,2)} = \frac{1}{2}(|00\rangle + |01\rangle + |10\rangle - |11\rangle)$. Now, let us perform the teleportation protocol for the single-qubit message $|M\rangle = \alpha|0\rangle + \beta|1\rangle$ via the two-qubit cluster state, the combined state after taking the tensor product of $|M\rangle$ and $|\psi_1\rangle$. Now, Alice applies the Bell basis measurement on her first and second qubit, that is $CX(1, 2)$, $H(1)$ and other operation $H(3)$ on the third qubit, given in circuit (Figure 5), and the final state is shown by Equation (4),

$$
\begin{aligned}
|\xi\rangle &= |M\rangle_1 \otimes |\psi_1\rangle_{23} \\
&= \frac{|00\rangle_{12}}{2}(\alpha|0\rangle + \beta|1\rangle)_3 + \frac{|01\rangle_{12}}{2}(\alpha|1\rangle + \beta|0\rangle)_3 \\
&\quad + \frac{|10\rangle_{12}}{2}(\alpha|0\rangle - \beta|1\rangle)_3 + \frac{|11\rangle_{12}}{2}(\alpha|1\rangle - \beta|0\rangle)_3
\end{aligned} \tag{4}
$$

At this stage of the protocol, teleportation of the message $|M\rangle$ to Bob's qubit has been done successfully. Now, Bob has to apply appropriate unitary operations on his qubit to recover the message. The controlled operations that Bob needs to apply on his qubit in the case of $|\psi_1\rangle = \frac{1}{2}(|00\rangle + |01\rangle + |10\rangle - |11\rangle)$ are shown by the quantum circuit (Figure 5) after the red colour dashed line. Choosing all combinations of $|a\rangle$ and $|b\rangle$, we get four types of two-qubit cluster state channels, shown in Table 5. Also, the teleportation is performed for each of the two-qubit cluster state channels, and the quantum cost is calculated, which is represented in the last column of Table 5. The controlled operations that Bob needs to apply on his qubit to recover the teleported message in all cases are shown in Table 6.

2.2.4 | Teleportation using three-qubit cluster state channel

The three-qubit cluster state is shared by three parties: Alice, Charlie and Bob. Here, Charlie acts as an extra controller in the teleportation. The three-qubit cluster state channel is given by the expression $|\psi\rangle = (|a\rangle|b\rangle|c\rangle)_{CZ(1,2)CZ(2,3)}$, where $|a\rangle, |b\rangle, |c\rangle \in \{|+\rangle, |-\rangle\}$. Taking $|a\rangle = |+\rangle$, $|b\rangle = |+\rangle$ and $|c\rangle = |+\rangle$, one of the eight three-qubit cluster states is given in Equation (5),

$$\begin{aligned}|\psi_1\rangle &= (|+\rangle|+\rangle|+\rangle)_{CZ(1,2)CZ(2,3)} \\ &= \frac{1}{2\sqrt{2}}\big(|000\rangle + |001\rangle + |010\rangle - |011\rangle + |100\rangle + |101\rangle \\ &\quad - |110\rangle + |111\rangle\big)\end{aligned} \tag{5}$$

Now, to perform the teleportation protocol for a single-qubit message $|M\rangle = \alpha|0\rangle + \beta|1\rangle$ via the three-qubit cluster state channel, the combined state after taking the tensor product of $|M\rangle$ and $|\psi_1\rangle$. Now, Alice applies the Bell basis measurement on the first and second qubit, that is $CX(1, 2)$ and $H(1)$ and other operation $H(3)$ on the third qubit as depicted in the quantum circuit shown in Figure 6. The final state is shown by Equation (6),

$$\begin{aligned}|\xi\rangle &= |M\rangle_1 \otimes |\psi_1\rangle_{234} \\ &= \frac{|00\rangle_{12}}{2}\big(|0\rangle_3(\alpha|0\rangle + \beta|1\rangle)_4 + |1\rangle_3(\alpha|1\rangle + \beta|0\rangle)_4\big) \\ &\quad + \frac{|01\rangle_{12}}{4}\big(|0\rangle_3(\alpha|1\rangle + \beta|0\rangle)_4 + |1\rangle_3(\alpha|0\rangle + \beta|1\rangle)_4\big) \\ &\quad + \frac{|10\rangle_{12}}{4}\big(|0\rangle_3(\alpha|0\rangle - \beta|1\rangle)_4 + |1\rangle_3(\alpha|1\rangle - \beta|0\rangle)_4\big) \\ &\quad + \frac{|11\rangle_{12}}{4}\big(|0\rangle_3(\alpha|1\rangle - \beta|0\rangle)_4 + |1\rangle_3(\alpha|0\rangle - \beta|1\rangle)_4\big)\end{aligned} \tag{6}$$

After reaching this state, the message $|M\rangle = \alpha|0\rangle + \beta|1\rangle$ is successfully teleported to Bob's qubit. Now, Bob needs to apply the appropriate unitary operations on his qubit to recover the message. The teleportation protocol is shown in the following quantum circuit (Figure 6). Here $|a\rangle, |b\rangle, |c\rangle \in \{|0\rangle, |1\rangle\}$. Choosing all the eight combinations of qubits $|a\rangle$, $|b\rangle$ and $|c\rangle$ we get eight different forms of three-qubit cluster states, which are shown in Table 7. Also, the teleportation protocol is performed for each of the eight channels, and the quantum cost is calculated, which is represented in the last column of Table 7. The controlled operations that Bob needs to apply on his qubit to recover the message in all the eight three-qubit cluster state entangled channels are given in Table 8.

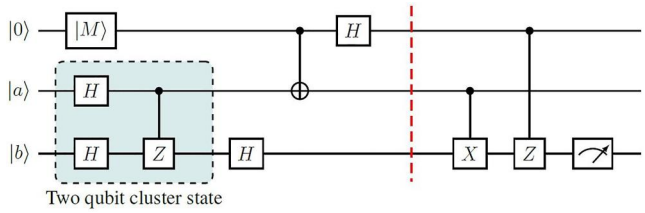

FIGURE 5 The teleportation protocol for teleporting a single-qubit message $|M\rangle = \alpha|0\rangle + \beta|1\rangle$ via the two-qubit cluster state; controlled operations are represented for $|\psi_1\rangle$ (given in Table 5) after the red dashed line, which will vary for different two-qubit cluster states

TABLE 5 The two-qubit cluster states, after choosing different values of $|a\rangle$ and $|b\rangle$

$\|a\rangle$	$\|b\rangle$	Two-qubit cluster state	Quantum cost
$\|0\rangle$	$\|0\rangle$	$\|\psi_1\rangle = \frac{1}{2}(\|00\rangle + \|01\rangle + \|10\rangle - \|11\rangle$	13
$\|0\rangle$	$\|1\rangle$	$\|\psi_2\rangle = \frac{1}{2}(\|00\rangle - \|01\rangle + \|10\rangle + \|11\rangle$	15
$\|1\rangle$	$\|0\rangle$	$\|\psi_3\rangle = \frac{1}{2}(\|00\rangle + \|01\rangle - \|10\rangle + \|11\rangle$	15
$\|1\rangle$	$\|1\rangle$	$\|\psi_4\rangle = \frac{1}{2}(\|00\rangle - \|01\rangle - \|10\rangle - \|11\rangle$	17

Note: The last column contains the quantum cost for teleporting a single-qubit message via the two-qubit cluster states.

TABLE 6 Controlled operations that Bob needs to apply to recover the teleported message via all the possible two-qubit cluster states

	Control operations			
Alice's measurement	$\|\psi_1\rangle$	$\|\psi_2\rangle$	$\|\psi_3\rangle$	$\|\psi_4\rangle$
$\|00\rangle$	$\mathbb{I}$	$\mathbb{X}$	$\mathbb{Z}$	$\mathbb{Z}$
$\|01\rangle$	$\mathbb{X}$	$\mathbb{I}$	$\mathbb{ZX}$	$\mathbb{ZX}$
$\|10\rangle$	$\mathbb{Z}$	$\mathbb{ZX}$	$\mathbb{I}$	$\mathbb{X}$
$\|11\rangle$	$\mathbb{ZX}$	$\mathbb{Z}$	$\mathbb{X}$	$\mathbb{I}$

2.2.5 | Teleportation using Brown et al. state [56]

Alice starts with a five-qubit entangled state called Brown et al. state, which is considered to be a maximally entangled five-qubit state showing a high degree of entanglement [57]. It was verified by Borras et al. [58] that Brown et al. state is highly efficient for teleportation. The state can be described by Equation (7) as follows:

$$|\psi\rangle = \frac{1}{2}[|001\rangle|\phi^-\rangle + |010\rangle|\psi^-\rangle + |100\rangle|\phi^+\rangle + |111\rangle|\psi^+\rangle] \tag{7}$$

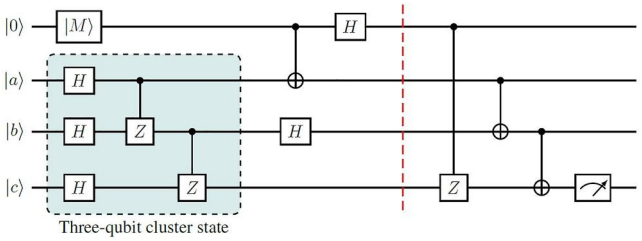

FIGURE 6 The teleportation protocol for teleporting a single-qubit message $|M\rangle = \alpha|0\rangle + \beta|1\rangle$ via the three-qubit cluster state; controlled operations are represented for $|\psi_1\rangle$ (given in Table 7) after the red dashed line, which will vary for different three-qubit cluster states

TABLE 7 Three-qubit cluster states after choosing different combinations of $|a\rangle$, $|b\rangle$ and $|c\rangle$

$\|a\rangle$	$\|b\rangle$	$\|c\rangle$	Three-qubit cluster states	Quantum cost
$\|0\rangle$	$\|0\rangle$	$\|0\rangle$	$\|\psi_1\rangle = \frac{1}{\sqrt{2}}(\|000\rangle + \|001\rangle + \|010\rangle - \|011\rangle + \|100\rangle + \|101\rangle - \|110\rangle + \|111\rangle)$	18
$\|0\rangle$	$\|0\rangle$	$\|1\rangle$	$\|\psi_2\rangle = \frac{1}{\sqrt{2}}(\|000\rangle - \|001\rangle + \|010\rangle + \|011\rangle + \|100\rangle - \|101\rangle - \|110\rangle - \|111\rangle)$	20
$\|0\rangle$	$\|1\rangle$	$\|0\rangle$	$\|\psi_3\rangle = \frac{1}{\sqrt{2}}(\|000\rangle + \|001\rangle - \|010\rangle + \|011\rangle + \|100\rangle + \|101\rangle + \|110\rangle - \|111\rangle)$	20
$\|0\rangle$	$\|1\rangle$	$\|1\rangle$	$\|\psi_4\rangle = \frac{1}{\sqrt{2}}(\|000\rangle - \|001\rangle - \|010\rangle - \|011\rangle + \|100\rangle - \|101\rangle + \|110\rangle + \|111\rangle)$	23
$\|1\rangle$	$\|0\rangle$	$\|0\rangle$	$\|\psi_5\rangle = \frac{1}{\sqrt{2}}(\|000\rangle + \|001\rangle + \|010\rangle - \|011\rangle - \|100\rangle - \|101\rangle + \|110\rangle - \|111\rangle)$	20
$\|1\rangle$	$\|0\rangle$	$\|1\rangle$	$\|\psi_6\rangle = \frac{1}{\sqrt{2}}(\|000\rangle - \|001\rangle + \|010\rangle + \|011\rangle - \|100\rangle + \|101\rangle + \|110\rangle + \|111\rangle)$	20
$\|1\rangle$	$\|1\rangle$	$\|0\rangle$	$\|\psi_7\rangle = \frac{1}{\sqrt{2}}(\|000\rangle + \|001\rangle - \|010\rangle + \|011\rangle - \|100\rangle - \|101\rangle - \|110\rangle + \|111\rangle)$	23
$\|1\rangle$	$\|1\rangle$	$\|1\rangle$	$\|\psi_8\rangle = \frac{1}{\sqrt{2}}(\|000\rangle - \|001\rangle - \|010\rangle - \|011\rangle - \|100\rangle + \|101\rangle - \|110\rangle - \|111\rangle)$	22

Note: The last column contains the quantum cost for teleportation of a single-qubit message via different three-qubit cluster states.

TABLE 8 The controlled operations that Bob needs to apply to recover the teleported message $|M\rangle = \alpha|0\rangle + \beta|1\rangle$ via all the eight three-qubit cluster states

Alice's measurement (Qubit{1,2})	Charlie's measurement Qubit{3}	Bob's operation (Qubit{4})							
		$\|\psi_1\rangle$	$\|\psi_2\rangle$	$\|\psi_3\rangle$	$\|\psi_4\rangle$	$\|\psi_5\rangle$	$\|\psi_6\rangle$	$\|\psi_7\rangle$	$\|\psi_8\rangle$
$\|00\rangle$	$\|0\rangle$	$\mathbb{I}$	$\mathbb{Z}$	$\mathbb{X}$	$\mathbb{I}$	$\mathbb{Z}$	$\mathbb{ZX}$	$\mathbb{ZX}$	$\mathbb{Z}$
	$\|1\rangle$	$\mathbb{Z}$	$\mathbb{ZX}$	$\mathbb{ZX}$	$\mathbb{Z}$	$\mathbb{I}$	$\mathbb{X}$	$\mathbb{X}$	$\mathbb{I}$
$\|01\rangle$	$\|0\rangle$	$\mathbb{X}$	$\mathbb{I}$	$\mathbb{I}$	$\mathbb{X}$	$\mathbb{ZX}$	$\mathbb{Z}$	$\mathbb{Z}$	$\mathbb{ZX}$
	$\|1\rangle$	$\mathbb{ZX}$	$\mathbb{Z}$	$\mathbb{Z}$	$\mathbb{ZX}$	$\mathbb{X}$	$\mathbb{I}$	$\mathbb{I}$	$\mathbb{X}$
$\|10\rangle$	$\|0\rangle$	$\mathbb{Z}$	$\mathbb{ZX}$	$\mathbb{ZX}$	$\mathbb{Z}$	$\mathbb{I}$	$\mathbb{X}$	$\mathbb{X}$	$\mathbb{I}$
	$\|1\rangle$	$\mathbb{I}$	$\mathbb{X}$	$\mathbb{X}$	$\mathbb{I}$	$\mathbb{Z}$	$\mathbb{ZX}$	$\mathbb{ZX}$	$\mathbb{Z}$
$\|11\rangle$	$\|0\rangle$	$\mathbb{ZX}$	$\mathbb{Z}$	$\mathbb{Z}$	$\mathbb{ZX}$	$\mathbb{X}$	$\mathbb{I}$	$\mathbb{I}$	$\mathbb{X}$
	$\|1\rangle$	$\mathbb{X}$	$\mathbb{I}$	$\mathbb{I}$	$\mathbb{X}$	$\mathbb{ZX}$	$\mathbb{Z}$	$\mathbb{Z}$	$\mathbb{ZX}$

where $|\phi^{\pm}\rangle = \frac{1}{\sqrt{2}}(|01\rangle \pm |10\rangle)$ and $|\psi^{\pm}\rangle = \frac{1}{\sqrt{2}}(|00\rangle \pm |11\rangle)$. Now, the teleportation of a single-qubit message $|M\rangle$ is to be performed using the Brown et al. state, $|\psi\rangle_{23456}$. So, the tensor product of message qubit $|M\rangle$ and the Brown et al. state $|\psi\rangle$ is taken, followed by some unitary operations, which are represented in the circuit described in Figure 7. Alice applies the Bell basis measurement on the first and second qubit, that is $CX(1,2)$ and $H(1)$ and the other operation described in Figure 7 on the last four qubits; the final state is given by Equation (8).

$$
\begin{aligned}
|\xi\rangle &= |M\rangle_1 \otimes |\psi_1\rangle_{2345} \\
&= \frac{|00\rangle_{12}}{4}\left(|011\rangle_{345}(\alpha|0\rangle + \beta|1\rangle)_6 + |100\rangle_{345}(\alpha|1\rangle\right. \\
&\quad \left. + \beta|0\rangle)_6\right) + \frac{|01\rangle_{12}}{4}\left(|011\rangle_{345}(\alpha|1\rangle + \beta|0\rangle)_6\right. \\
&\quad \left. + |100\rangle_{345}(\alpha|0\rangle + \beta|1\rangle)_6\right) + \frac{|10\rangle_{12}}{4}\left(|011\rangle_{345}(\alpha|0\rangle\right. \\
&\quad \left. - \beta|1\rangle)_6 + |100\rangle_{345}(\alpha|1\rangle - \beta|0\rangle)_6\right) + \frac{|11\rangle_{12}}{4} \\
&\quad \left(|011\rangle_{345}(\alpha|1\rangle - \beta|0\rangle)_6 + |100\rangle_{345}(\alpha|0\rangle - \beta|1\rangle)_6\right) \qquad (8)
\end{aligned}
$$

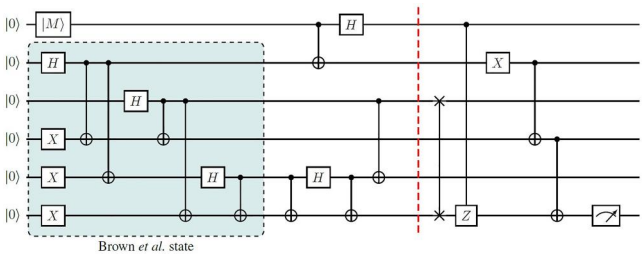

FIGURE 7 Teleportation protocol for teleporting a single-qubit message $|M\rangle = \alpha|0\rangle + \beta|1\rangle$ via Brown et al. state; the controlled operations are represented after the red dashed line

After the message qubit $|M\rangle = \alpha|0\rangle + \beta|1\rangle$ is teleported to Bob's qubit, Bob needs to apply appropriate unitary operations on his qubit to recover the message successfully using the Brown et al. state, which are shown in Table 9 and represented in the quantum circuit (Figure 7) after the red dashed line. The quantum cost for teleporting the single-qubit secret message via Brown et al. state is 24.

2.2.6 | Teleportation using Borras et al. state

Borras et al. introduced a highly entangled six-qubit quantum state, which is not decomposable into product of Bell states [58]. Borras et al. state exhibits genuine entanglement according to many measures. Also, no other six-qubit pure state has been found that evolves to a mixed state with a higher amount of entanglement [59]. The Borras et al. state can be written in the terms of Bell basis given by Equation (9).

$$\begin{aligned}|\psi\rangle = \frac{1}{4}(&|000\rangle(|0\rangle|\psi^+\rangle + |1\rangle|\phi^+\rangle) + |001\rangle(|0\rangle|\phi^-\rangle \\ &- |1\rangle|\psi^-\rangle) + |010\rangle(|0\rangle|\phi^+\rangle - |1\rangle|\psi^+\rangle) \\ &+ |011\rangle(|0\rangle|\psi^-\rangle + |1\rangle|\phi^-\rangle) + |100\rangle(-|0\rangle|\phi^-\rangle \\ &- |1\rangle|\psi^-\rangle) + |101\rangle(-|0\rangle|\psi^+\rangle + |1\rangle|\phi^+\rangle) \\ &+ |110\rangle(|0\rangle|\psi^-\rangle - |1\rangle|\phi^-\rangle) \\ &+ |111\rangle(|0\rangle|\phi^+\rangle + |1\rangle|\psi^+\rangle)) \end{aligned} \tag{9}$$

where $|\phi^\pm\rangle = \frac{1}{\sqrt{2}}(|01\rangle \pm |10\rangle)$ and $|\psi^\pm\rangle = \frac{1}{\sqrt{2}}(|00\rangle \pm |11\rangle)$. To teleport the single-qubit message $|M\rangle = \alpha|0\rangle + \beta|1\rangle$ via Borras et al. state channel, the combined state after taking the tensor product of $|M\rangle$ and $|\psi\rangle$ is given in Equation (10).

$$\begin{aligned}|\xi\rangle &= |M\rangle_1 \otimes |\psi\rangle_{234567} \\ &= (\alpha|0\rangle + \beta|1\rangle)_1 \otimes \frac{1}{4}(|000\rangle(|0\rangle|\psi^+\rangle + |1\rangle|\phi^+\rangle) \\ &\quad + |001\rangle(|0\rangle|\phi^-\rangle - |1\rangle|\psi^-\rangle) + |010\rangle(|0\rangle|\phi^+\rangle \\ &\quad - |1\rangle|\psi^+\rangle) + |011\rangle(|0\rangle|\psi^-\rangle + |1\rangle|\phi^-\rangle) \\ &\quad + |100\rangle(-|0\rangle|\phi^-\rangle - |1\rangle|\psi^-\rangle) + |101\rangle(-|0\rangle|\psi^+\rangle \\ &\quad + |1\rangle|\phi^+\rangle) + |110\rangle(|0\rangle|\psi^-\rangle - |1\rangle|\phi^-\rangle) \\ &\quad + |111\rangle(|0\rangle|\phi^+\rangle + |1\rangle|\psi^+\rangle))_{234567} \end{aligned} \tag{10}$$

Now, Alice applies the Bell basis measurement on the first and second qubit, that is $CX(1, 2)$ and $H(1)$ and other operations on the last five qubits depicted in quantum circuit (Figure 8); the final state of the system is given in Equation (11),

$$\begin{aligned}|\xi\rangle = &\frac{|00\rangle_{12}}{2}\left(|0000\rangle_{3456}(\alpha|0\rangle + \beta|1\rangle)_7 + |1001\rangle_{3456}\right. \\ &\times \left.(\alpha|1\rangle - \beta|0\rangle)_7\right) + \frac{|01\rangle_{12}}{4}\left(|0000\rangle_{3456}(\alpha|1\rangle + \beta|0\rangle)_7\right. \\ &+ \left.|1001\rangle_{3456}(-\alpha|0\rangle + \beta|1\rangle)_7\right) + \frac{|10\rangle_{12}}{4}\left(|0000\rangle_{3456}\right. \\ &\times (\alpha|0\rangle - \beta|1\rangle)_7 + |1001\rangle_{3456}(\alpha|1\rangle + \beta|0\rangle)_7\Big) \\ &+ \frac{|11\rangle_{12}}{4}\left(|0000\rangle_{3456}(\alpha|1\rangle - \beta|0\rangle)_7 + |1001\rangle_{3456}\right. \\ &\times \left.(\alpha|0\rangle + \beta|1\rangle)_7\right) \end{aligned} \tag{11}$$

After reaching this state, Bob applies proper unitary operations on the seventh qubit to recover the teleported message. The unitary operations are shown in Table 10. The teleportation protocol is given in the following quantum circuit (Figure 8). The quantum cost for teleporting the single-qubit message via Borras et al. state is 38.

3 | STUDY OF EFFECT OF NOISY ENVIRONMENT

Practically, it is impossible to perform quantum teleportation without noise in the entangled channel. The best we can do is to study the sources and effects of noise in our system and minimise them up to best possible extent. Here, we conveniently study the impact of six different kinds of noise present in all the teleportation protocols discussed earlier. We do this

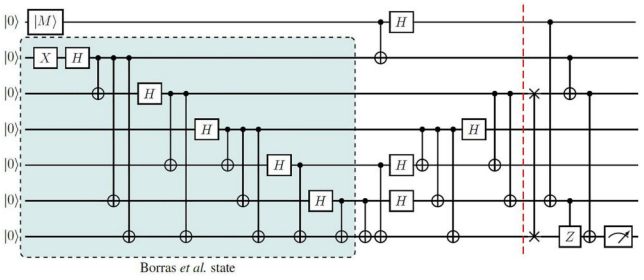

FIGURE 8 Teleportation protocol of a single-qubit message $|M\rangle = \alpha|0\rangle + \beta|1\rangle$ using Borras et al. state; the controlled operations are represented after the red dashed line

TABLE 9 The controlled operations that Bob needs to apply to recover the teleported message $|M\rangle = \alpha|0\rangle + \beta|1\rangle$ via Brown et al. state

Alice's measurement (Qubit{1,2})	Qubit{3,4,5}	Last qubit measurement (Qubit{6})	Control operations
$\|00\rangle_{12}$	$\|110\rangle_{345}$	$\alpha\|0\rangle + \beta\|1\rangle$	$\mathbb{I}$
	$\|011\rangle_{345}$	$\alpha\|1\rangle + \beta\|0\rangle$	$\mathbb{X}$
$\|01\rangle_{12}$	$\|110\rangle_{345}$	$\alpha\|1\rangle + \beta\|0\rangle$	$\mathbb{X}$
	$\|011\rangle_{345}$	$\alpha\|0\rangle + \beta\|1\rangle$	$\mathbb{I}$
$\|10\rangle_{12}$	$\|110\rangle_{345}$	$\alpha\|0\rangle - \beta\|1\rangle$	$\mathbb{Z}$
	$\|011\rangle_{345}$	$\alpha\|1\rangle - \beta\|0\rangle$	$\mathbb{ZX}$
$\|11\rangle_{12}$	$\|110\rangle_{345}$	$\alpha\|1\rangle - \beta\|0\rangle$	$\mathbb{ZX}$
	$\|011\rangle_{345}$	$\alpha\|0\rangle - \beta\|1\rangle$	$\mathbb{Z}$

TABLE 10 Controlled operations that Bob needs to apply to recover the teleported message via Borras et al. state

Alice's measurement (Qubit{1,2})	Qubit {3,4,5,6}	Last qubit measurement (Qubit{7})	Control operations
$\|00\rangle_{12}$	$\|0000\rangle_{3456}$	$\alpha\|0\rangle + \beta\|1\rangle$	$\mathbb{I}$
	$\|0011\rangle_{3456}$	$\alpha\|1\rangle - \beta\|0\rangle$	$\mathbb{ZX}$
$\|01\rangle_{12}$	$\|0000\rangle_{3456}$	$\alpha\|1\rangle + \beta\|0\rangle$	$\mathbb{X}$
	$\|0011\rangle_{3456}$	$-\alpha\|0\rangle + \beta\|1\rangle$	$\mathbb{Z}$
$\|10\rangle_{12}$	$\|0000\rangle_{3456}$	$\alpha\|0\rangle - \beta\|1\rangle$	$\mathbb{Z}$
	$\|0011\rangle_{3456}$	$\alpha\|1\rangle + \beta\|0\rangle$	$\mathbb{X}$
$\|11\rangle_{12}$	$\|0000\rangle_{3456}$	$\alpha\|1\rangle - \beta\|0\rangle$	$\mathbb{ZX}$
	$\|0011\rangle_{3456}$	$\alpha\|0\rangle + \beta\|1\rangle$	$\mathbb{I}$

by checking the evolution of the density matrix $\rho = |\psi\rangle\langle\psi|$ under the effect of Kraus operators. Using the operator sum representation, the interaction of noise in the quantum channel can be represented with the help of Kraus operators E_k. The action of noise on a particular qubit k is described by the density matrix ρ_k as given by Equation (12).

$$\xi^r(\rho_k) = \sum_{j=1}^{n} (E_j)\ \rho_k\ (E_j)^\dagger \tag{12}$$

where $r \in \{B, W, F, A, P, D\}$ for bit-flip, phase-flip, bit-phase-flip, amplitude damping, phase damping and depolarising damping, respectively.

$$j \in \begin{cases} \{0,1\} & \text{for} \quad r = B, W, F, A \\ \{0,1,2\} & \text{for} \quad r = P \\ \{0,1,2,3\} & \text{for} \quad r = D \end{cases}$$

In the noisy environment, the shared entangled state would become a mixed state after the distribution of the qubits. To recover the original message, Bob has to make appropriate unitary operations on his own qubit. The final state ρ^r_{out} can be expressed in terms of the density matrix as shown in Equation (13).

$$\rho^r_{out} = Tr_{i_1 i_2 \ldots i_{n-1}}\left\{\mathbb{U}\left[\rho_k \otimes \xi^r(\rho_l)\right]\mathbb{U}^\dagger\right\} \tag{13}$$

where $Tr_{i_1 i_2 \ldots i_{n-1}}$ is the partial trace over the qubits $i_1, i_2, \ldots, i_{n-1}$ and $\mathbb{U}$ is the unitary operator to describe the teleportation process, which is given by Equation (14),

$$\begin{aligned}\mathbb{U} = &\left\{\mathbb{I}_1 \otimes \mathbb{I}_2 \otimes \ldots \mathbb{I}_{n-1} \otimes \sigma_n^{i_1 i_2 \ldots i_{n-1}}\right\} \\ &\left\{|\phi\rangle_{12}\langle\phi|_{12} \otimes \mathbb{I}_3 \ldots \otimes \mathbb{I}_n\right\}\left\{\mathbb{I}_1 \otimes \mathbb{I}_2 \ldots U_{j_1 j_2} \ldots \otimes \mathbb{I}_n\right\} \\ &\left\{\mathbb{I}_1 \otimes \mathbb{I}_2 \ldots U_{k_1} \ldots \otimes \mathbb{I}_n\right\}\end{aligned} \tag{14}$$

where $\sigma_n^{i_1 i_2 \ldots i_{n-1}}$ is the unitary operators for recovery of Bob's qubit. Then $|\phi\rangle_{12}\langle\phi|_{12}$ is the Bell basis measurement on the first two qubits, $U_{j_1 j_2}$ represents the CNOT gate from qubit j_1 to j_2 and U_{k_1} represents the unitary gate on qubit k_1. Depending upon the different choices of the entangled channel, these unitary operations change. Now, the effect of noise in the entangled channel can be visualised by calculating the fidelity between the initial single-qubit message $|\psi\rangle$ and the density matrix ρ^r_{out}. Fidelity represents the closeness of the two quantum states, and it gives a mathematical prescription for the quantification of the degree of similarity of a pair of quantum states [60]. The mathematical expression for fidelity is given by Equation (15).

$$F = \langle\Psi|\rho^r_{out}|\Psi\rangle \tag{15}$$

Some quantum state information will be lost during the teleportation through a noisy environment, so fidelity is a perfect metric to measure how much information is lost. If the fidelity $F = 1$, then this indicates the ideal case where no information is lost, and the teleportation is perfect. Meanwhile, $F = 0$ implies that all the information is lost, and the quantum states before and after the teleportation are orthogonal. Thus, the fidelity ranges between 0 and 1. We now discuss the effects of six types of noise (bit-flip, phase-flip, bit-phase-flip, amplitude damping, phase damping, and depolarising noise) in this section.

3.1 | Bit-flip noisy environment

In the presence of bit-flip noise, the quantum state $|0\rangle$ is changed to $|1\rangle$ and vice-versa with probability η_B, and the qubits remain unchanged with the probability $(1 - \eta_B)$ [52, 61]. Its operations on a qubit can be described by Kraus operators given by Equation (16) as follows:

$$\begin{aligned} E_0^B &= \sqrt{1-\eta_B}\ \ \mathbb{I} = \sqrt{1-\eta_B}\begin{pmatrix} 1 & 0 \\ 0 & 1 \end{pmatrix}, \\ E_1^B &= \sqrt{\eta_B}\ \ \mathbb{X} = \sqrt{\eta_B}\begin{pmatrix} 0 & 1 \\ 1 & 0 \end{pmatrix} \end{aligned} \tag{16}$$

where $0 \leq \eta_B \leq 1$ represents the bit-flip error probability, which describes the probability of occurring error in the quantum state due to transmitted qubit. The effects of bit-flip noise on the six entangled channels can be seen by evaluating the affected density matrix after the introduction of noise. The affected density matrices under the bit-flip noise for all the six channels, the Bell channel, GHZ channel, two-qubit cluster state, three-qubit cluster state, Brown et al. state and the Borras et al., are denoted by $\mathcal{E}_1^B(\rho), \mathcal{E}_2^B(\rho), \mathcal{E}_3^B(\rho), \mathcal{E}_4^B(\rho), \mathcal{E}_5^B(\rho), \mathcal{E}_6^B(\rho)$, respectively. The expression for these matrices are given in Equations (A1) to (A6) in Appendix A.

3.2 | Phase-flip noisy environment

In the presence of phase-flip noise, the phase of the qubit changes from $|1\rangle$ to $-|1\rangle$, and it remains unchanged if the qubit is $|0\rangle$. Its Kraus operators [52, 61] are given by Equation (17),

$$E_0^W = \sqrt{1-\eta_W}\ \ \mathbb{I} = \sqrt{1-\eta_W}\begin{pmatrix} 1 & 0 \\ 0 & 1 \end{pmatrix},$$
$$E_1^W = \sqrt{\eta_W}\ \ \mathbb{Z} = \sqrt{\eta_W}\begin{pmatrix} 1 & 0 \\ 0 & -1 \end{pmatrix}. \quad (17)$$

where $0 \leq \eta_W \leq 1$ represents the phase-flip error probability, which describes the possibility of occurring error in the quantum state due to transmitted qubit. The effect of phase-flip noise on the six entangled channels can be seen by evaluating the affected density matrix after noise has been introduced in the channel, and the affected density matrices under the phase-flip noise for all the six channels are given in Equations (A8) to (A13) in Appendix A.

3.3 | Bit-phase-flip noisy environment

The Kraus operators of bit-phase-flip are given by the following matrices [52, 61]:

$$E_0^F = \sqrt{1-\eta_F}\ \ \mathbb{I} = \sqrt{1-\eta_F}\begin{pmatrix} 1 & 0 \\ 0 & 1 \end{pmatrix},$$
$$E_1^F = \sqrt{\eta_F}\ \ \mathbb{Y} = \sqrt{\eta_F}\begin{pmatrix} 0 & -i \\ i & 0 \end{pmatrix} \quad (18)$$

where $0 \leq \eta_F \leq 1$ represents the bit-phase-flip error probability, which describes the possibility of occurring error in quantum state due to travel qubit. The effect of bit-phase-flip noise on the six entangled channels can be seen by evaluating the affected density matrix after noise has been introduced in the channel, and the affected density matrices under the bit-phase flip noise for all the six channels are given in Equations (A15) to (A20) in Appendix A.

3.4 | Effect of amplitude damping (AD) noise

The process of amplitude damping is an essential concept in modelling the energy dissipation in several quantum systems, and the following matrices give their Kraus operators [52, 61].

$$E_0^A = \begin{pmatrix} 1 & 0 \\ 0 & \sqrt{1-\eta_A} \end{pmatrix}, \quad E_1^A = \begin{pmatrix} 0 & \sqrt{\eta_A} \\ 0 & 0 \end{pmatrix} \quad (19)$$

where $0 \leq \eta_A \leq 1$ represents the decoherence rate of amplitude damping, which describes the possibility of occurring error in the quantum state due to travel qubit. The effect of amplitude damping on the six entangled channels can be seen by evaluating the affected density matrices after the noise has been introduced in the channel; the affected density matrices under the amplitude damping noise for all the six entangled channels are given in Equations (A21) to (A26) in Appendix A.

3.5 | Phase damping noisy environment

Phase damping involves loss of information about relative phases in a quantum state. During phase damping, the principal quantum system becomes entangled with the environment [1]. The Kraus operators $\{E_0^P, E_1^P, E_2^P\}$ for phase damping noise can be described in Equation (20) [52, 61].

$$E_0^P = \sqrt{1-\eta_P}\begin{pmatrix} 1 & 0 \\ 0 & 1 \end{pmatrix}, \quad E_1^P = \begin{pmatrix} \sqrt{\eta_P} & 0 \\ 0 & 0 \end{pmatrix},$$
$$E_2^P = \begin{pmatrix} 0 & 0 \\ 0 & \sqrt{\eta_P} \end{pmatrix} \quad (20)$$

where $0 \leq \eta_P \leq 1$ represents the decoherence rate of phase damping, which describes the possibility of occurring error in quantum state due to travel qubit. The effect of phase damping on the six entangled channels can be seen by evaluating the affected density matrices after noise has been introduced in the channel, the affected density matrices under the phase damping noise for all the six entangled channels are given in Equations (A27) to (A32) in Appendix A.

3.6 | Depolarising noisy environment

In depolarising noisy environment, the qubits of the quantum state are depolarised with probability η_D and the qubits are left invariant with probability $1 - \eta_D$. The Pauli operators $\mathbb{X}, \mathbb{Y}$ and $\mathbb{Z}$ act on the qubits with probability $\eta_D/3$. The following matrices give the Kraus operators [52, 61].

$$E_0^D = \sqrt{1-\eta_D}\begin{pmatrix} 1 & 0 \\ 0 & 1 \end{pmatrix}, \quad E_1^D = \sqrt{\frac{\eta_D}{3}}\begin{pmatrix} 0 & 1 \\ 1 & 0 \end{pmatrix},$$
$$E_2^D = \sqrt{\frac{\eta_D}{3}}\begin{pmatrix} 0 & -i \\ i & 0 \end{pmatrix}, \quad E_3^D = \sqrt{\frac{\eta_D}{3}}\begin{pmatrix} 1 & 0 \\ 0 & -1 \end{pmatrix} \quad (21)$$

The effect of depolarising noise on the six entangled channels can be seen by evaluating the affected density matrix after noise has been introduced in the channel, and the affected density matrices under the depolarising noise for all the six entangled channels are given in Equations (A33) to (A38) in Appendix A.

4 | DISCUSSION AND CONCLUSION

In this study, the quantum cost is calculated for all the teleportation protocols and shown in Figure 9. Here we observe that the quantum cost increases as the number of qubits in the entangled channels increases. For example, the quantum cost of the Borras et al. channel is the highest as the number of quantum gates required to teleport the information is greater than that of

the other entangled channels with a lower number of qubits. The computational complexity of a reversible gate can be represented by its quantum cost, so the higher the quantum cost, the more complexity in teleportation. The graphs plotted for different entangled channels show an upward trend as the number of qubits increases in the channel. In the case of the two-qubit cluster state channel and the three-qubit GHZ channel, the average quantum cost is the same, which means that the complexity of teleportation in these two entangled channels is the same. However, the average quantum cost in the case of a three-qubit GHZ channel is 15, whereas, that in the case of a three-qubit cluster state is 21. It means that the quantum cost may vary for different entangled states even with the same number of qubits. However, it will ultimately increase as the number of qubits increases in the entangled channel.

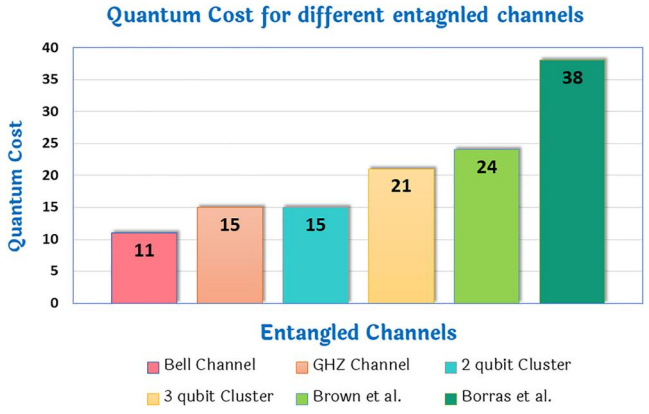

FIGURE 9 The quantum cost for different entangled channels. Average cost has been taken in case of Bell channel, Greenberger–Horne–Zeilinger channel, two-qubit cluster state and three-qubit cluster state channels

The effect of noise on the entangled channel is also studied. We have derived the density matrices of the teleported state, which is influenced by the noise. The fidelity provides the closeness between the two quantum states. The effect of bit-flip noise is visualised with the help of graphical representation of variation in the fidelity against the phase-flip noise parameter η_B given in Figure 10. From the graph, it is clear that fidelity decreases with the increase in the noise parameter $\eta_B \in [0, 0.5]$. After that, the fidelity shows an upward trend and reaches to 1 as $\eta_W \in [0.5, 1]$ in case of Bell channel, GHZ channel, three-qubit cluster sate, Brown et al. and Borras et al. However, in two-qubit cluster channel, the fidelity decreases rapidly to zero as the noise parameter $\eta_B \in [0.5, 1]$. The effect of phase-flip noise is visualised with the help of a graphical representation of variation in the fidelity against the bit-flip noise parameter η_W (see Figure 10). From the plot, it can be observed that fidelity decreases with the increase in the noise parameter $\eta_W \in [0, 0.5]$. After that, the fidelity shows an upward trend and reaches to 1 as $\eta_W \in [0.5, 1]$ in case of Bell channel, Brown et al. and Borras et al. However, in the other three channels viz. GHZ channel, two-qubit cluster state and three-qubit cluster state the fidelity increases but does not reaches to 1. In the case of bit-phase-flip noise, it is visualised with the help of a graphical representation of variation in the fidelity against the bit-phase-flip noise parameter η_F, which is given in Figure 10. From the plot, it is illustrated that fidelity decreases with the increase in the noise parameter $\eta_F \in [0, 0.5]$.

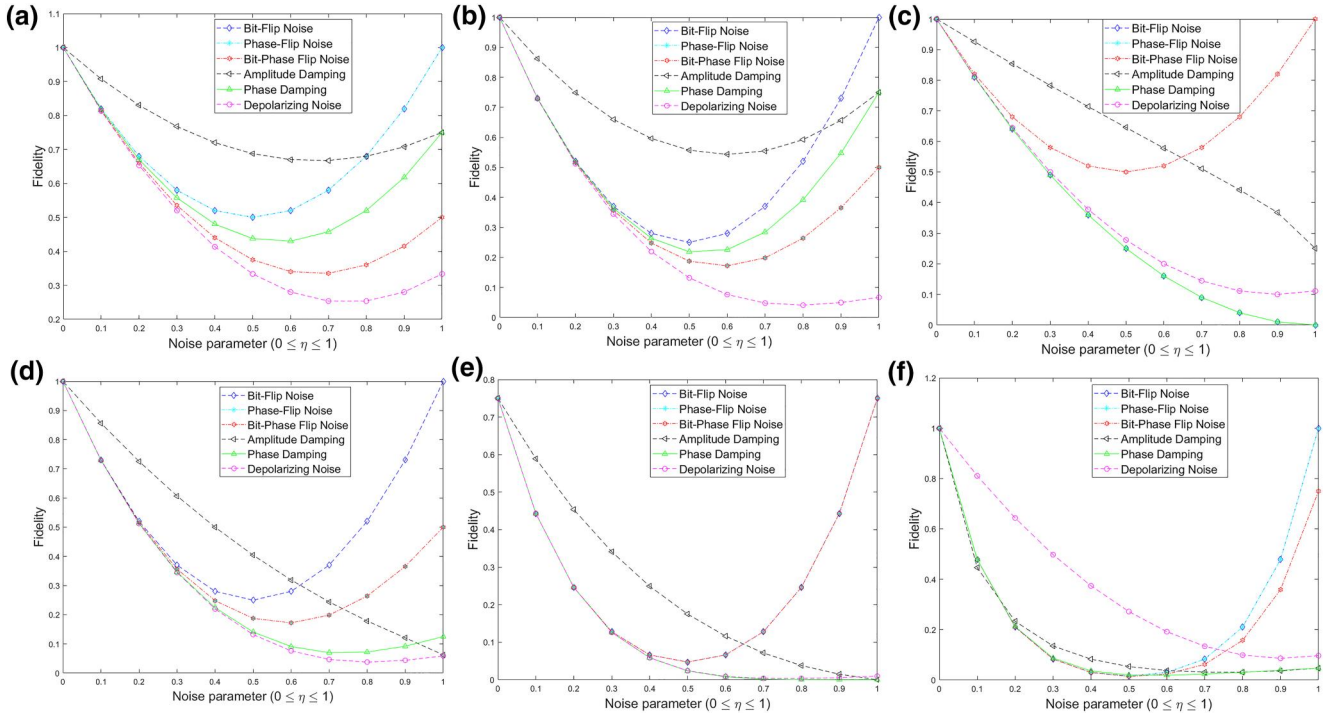

FIGURE 10 The effect of all six noises on the teleportation is visualised through a graphical representation of variation of fidelity against the noise parameter η. Here ($\eta \in \{\eta_B, \eta_W, \eta_F, \eta_A, \eta_P, \eta_D\}$ for bit-flip noise, phase-flip noise, bit-phase-flip noise, amplitude damping, phase damping and depolarising noise, respectively). The teleportation channels are (a) Bell channel (b) Greenberger–Horne–Zeilinger channel (c) Two-qubit cluster state channel (d) Three-qubit cluster state channel (e) Brown et al. channel and (f) Borras et al. channel

After that, the fidelity shows an upward trend and reaches to 1 as $\eta_F \in [0.5, 1]$ in the case of the two-qubit cluster state and Brown et al. However, in other entangled channels, it increases slowly but does not reach to 1 as the noise parameter increases in the range $\eta_F \in [0.5, 1]$. For amplitude damping noise, the graphical representation of variation in the fidelity against the amplitude damping noise parameter η_A is given in Figure 10. From the plot, it is illustrated that fidelity decreases with the increase in the noise parameter $\eta_A \in [0, 0.5]$, and after that the fidelity shows an upward trend as $\eta_A \in [0.5, 1]$ in the case of Bell channel and GHZ channel, but in all other entangled channels the fidelity decreases monotonically as the noise parameter increases in the range $\eta_A \in [0.5, 1]$, in fact it reaches zero for $\eta_A = 1$ in case of teleportation via Brown et al. state, represented in Figure 10e. For phase damping noise, the graphical representation of variation in the fidelity against the phase damping noise parameter η_P is given in Figure 10. From the plot, it is illustrated that fidelity decreases with the increase in the noise parameter $\eta_P \in [0, 0.5]$, and after that the fidelity shows an upward trend as $\eta_P \in [0.5, 1]$ in the case of Bell channel and GHZ channel and a slight increase in the case of three-qubit cluster state, as can be seen in Figure 10d. However, in all other entangled channels, the fidelity decreases monotonically as the noise parameter increases in the range $\eta_P \in [0.5, 1]$, in fact it reaches zero for $\eta_P = 1$ in case of teleportation via two-qubit cluster state and Brown et al. state. One more interesting observation is that the effect of phase-flip noise coincides with the bit-flip and phase-flip in the case of teleportation via the two-qubit cluster state, as can be seen in Figure 10c. For depolarising noise, the graphical representation of variation in the fidelity against the phase damping noise parameter η_D is given in Figure 10. From the plot, it is illustrated that fidelity decreases with the increase in the noise parameter $\eta_D \in [0, 0.5]$. After that, the fidelity shows a slight upward trend as $\eta_D \in [0.5, 1]$ in case of teleportation via Bell channel, as can be seen in Figure 10a. However, in all other entangled channels, the fidelity decreases monotonically as the noise parameter increases in the range $\eta_D \in [0.5, 1]$. In fact it reaches zero for $\eta_D = 1$ in case of teleportation via Borras et al. state. One more interesting observation is that the effect of depolarising noise coincides with the phase-flip noise in the case of teleportation via the Brown et al. state. In a nutshell, amplitude damping, phase damping and depolarising noise have the maximum impact on teleportation. It is cumbersome to perform its practical implementation on real quantum computers due to the non-unitary operators involved in the noise implementation process. However, this is attainable and could be achieved in the near future as a potential application.

ACKNOWLEDGEMENT

This work is partially supported by Department of Science and Technology, Ministry of Science and Technology, and Science and Engineering Research Board SERB/2020/002040. The authors would like to thank IBM for providing access to their QE cloud servers.

CONFLICT OF INTEREST

The authors declare that there is no conflict of interest that could be perceived as prejudicing the impartiality of the research reported.

DATA AVAILABILITY STATEMENT

The data that support the plots within this paper and other findings of this study are available from the corresponding authors upon reasonable request.

ORCID

Deepak Singh https://orcid.org/0000-0001-5598-5407
Sanjeev Kumar https://orcid.org/0000-0001-7728-3668
Bikash K. Behera https://orcid.org/0000-0003-2629-3377

REFERENCES

1. McMahon, D.: Quantum Computing Explained, pp. 254–271. Wiley, United States of America (2007)
2. Nielson, M., Chuang, I.: Quantum Computing and Quantum Information, pp. 356–385. Cambridge University Press, Cambridge (2000)
3. Yuan, X.X., et al.: Experimental demonstration of a quantum router. Sci. Rep. 5, 1–9 (2015). https://doi.org/10.1038/srep12452
4. Erhard, M., Malik, M., Zeilinger, A.: A quantum router for high-dimensional entanglement. Quantum Sci. Technol. 2(1), 014001 (2017). https://doi.org/10.1088/2058-9565/aa5917
5. Bartkiewicz, K., Černoch, A., Lemr, K.: Implementation of an efficient linear-optical quantum router. Sci. Rep. 8, 1–8 (2018). https://doi.org/10.1038/s41598-018-31273-0
6. Behera, B.K., et al.: Designing quantum router in IBM quantum computer. Quantum Inf. Process. 18(11), 1–13 (2019). https://doi.org/10.1007/s11128-019-2436-x
7. Briegel, H.J., et al.: Quantum repeaters for quantum communication. Epistemol. Exp. Perspect. Quantum Phys. 147–154 (1999). https://doi.org/10.1007/978-94-017-1454-9_11
8. Munro, W.J., et al.: Inside quantum repeaters. IEEE J. Sel. Top. Quant. Electron. 21(3), 78–90 (2015). https://doi.org/10.1109/jstqe.2015.2392076
9. Azuma, K., Tamaki, K., Lo, H.K.: All-photonic quantum repeaters. Nat. Commun. 6, 1–7 (2015). https://doi.org/10.1038/ncomms7787
10. Behera, B.K., et al.: Demonstration of entanglement purification and swapping protocol to design quantum repeater in IBM quantum computer. Quantum Inf. Process. 18(4), 1–13 (2019). https://doi.org/10.1007/s11128-019-2229-2
11. Ruihong, Q., Ying, M.: Research progress of quantum repeaters. J. Phys. 1237(5), 052032 (2019). https://doi.org/10.1088/1742-6596/1237/5/052032
12. Vallone, G., et al.: Experimental satellite quantum communications. Phys. Rev. Lett. 115(4), 040502 (2015). https://doi.org/10.1103/physrevlett.115.040502
13. Gibney, E.: Chinese satellite is one giant step for the quantum internet. Nat. News. 535(7613), 478–479 (2016). https://doi.org/10.1038/535478a
14. Wanisch, D., Fritzsche, S.: Driven spin chains as high-quality quantum routers. Phys. Rev. Lett. 102(3), 032624 (2020). https://doi.org/10.1103/physreva.102.032624
15. Gisin, N., et al.: Quantum cryptography. Rev. Mod. Phys. 74(1), 145–195 (2020). https://doi.org/10.1103/revmodphys.74.145
16. Bennett, C.H., et al.: Experimental quantum cryptography. J. Cryptol. 5(1), 3–28 (2020). https://doi.org/10.1007/bf00191318
17. Bennett, C.H.: Quantum cryptography using any two nonorthogonal states. Phys. Rev. Lett. 68(21), 3121–3124 (1992). https://doi.org/10.1103/physrevlett.68.3121
18. Das, D., et al.: Experimental detection of quantum information sharing and its quantification in quantum spin systems. New J. Phys. 15(1), 013047 (2013). https://doi.org/10.1088/1367-2630/15/1/013047

19. Zheng, S.B.: Splitting quantum information via W states. Phys. Rev. A. 74(5), 054303 (2006). https://doi.org/10.1103/physreva.74.054303
20. Muralidharan, S., Panigrahi, P.K.: Quantum-information splitting using multipartite cluster states. Phys. Rev. A. 78(6), 062333 (2008). https://doi.org/10.1103/physreva.78.062333
21. Musanna, F., Kumar, S.: A novel three-party quantum secret sharing scheme based on Bell state sequential measurements with application in quantum image sharing. Quantum Inf. Process. 19(10), 1–21 (2020). https://doi.org/10.1007/s11128-020-02854-8
22. Harrow, A., Hayden, P., Leung, D.: Superdense coding of quantum states. Phys. Rev. A. 92(18), 187901 (2004). https://doi.org/10.1103/physrevlett.92.187901
23. Xia, Y., Song, H.S.: Controlled quantum secure direct communication using a non-symmetric quantum channel with quantum superdense coding. Phys. Rev. A. 364(2), 117–122 (2007). https://doi.org/10.1016/j.physleta.2006.11.080
24. Bennett, C.H., et al.: Remote preparation of quantum states. IEEE Trans. Inf. Theor. 51(1), 56–74 (2005). https://doi.org/10.1109/tit.2004.839476
25. An, N.B., Choudhury, B.S., Samanta, S.: Two-way remote preparations of inequivalent quantum states under a common control. Int. J. Theor. Phys. 60(1), 47–62 (2021). https://doi.org/10.1007/s10773-020-04657-0
26. Shukla, C., Thapliyal, K., Pathak, A.: Hierarchical joint remote state preparation in noisy environment. Quantum Inf. Process. 16(8), 1–32 (2017). https://doi.org/10.1007/s11128-017-1654-3
27. Barik, S., et al.: Deterministic hierarchical remote state preparation of a two-qubit entangled state using Brown et al. state in a noisy environment. IET Quant. Commun. 1(2), 49–54 (2020). https://doi.org/10.1049/iet-qtc.2020.0005
28. Bennett, C.H., et al.: Teleporting an unknown quantum state via dual classical and Einstein-Podolsky-Rosen channels. Phys. Rev. Lett. 70(13), 1895–1899 (1993). https://doi.org/10.1103/physrevlett.70.1895
29. Bouwmeester, D., et al.: Experimental quantum teleportation. Nature. 390(6660), 575–579 (1993). https://doi.org/10.1038/37539
30. Wang, X.L., et al.: Quantum teleportation of multiple degrees of freedom of a single photon. Nature. 518(7540), 516–519 (2015). https://doi.org/10.1038/nature14246
31. Metcalf, B.J., et al.: Quantum teleportation on a photonic chip. Nature Photon. 8(10), 770–774 (2014). https://doi.org/10.1038/nphoton.2014.217
32. Zhou, R.G., Qian, C., Ian, H.: Bidirectional quantum teleportation of two-qubit state via four-qubit cluster state. Int. J. Theor. Phys. 58(1), 150–156 (2019). https://doi.org/10.1007/s10773-018-3919-8
33. Hu, T., et al.: Quantum teleportation and dense coding via topological basis. Quantum Inf. Process. 12(11), 3369–3381 (2013). https://doi.org/10.1007/s11128-013-0614-9
34. Riebe, M., et al.: Deterministic quantum teleportation with atoms. Nature. 429(6993), 734–737 (2004). https://doi.org/10.1038/nature02570
35. Li, Y.H., et al.: Splitting unknown two-qubit state using five-qubit entangled state. Int. J. Theor. Phys. 53(1), 111–115 (2014). https://doi.org/10.1007/s10773-013-1788-8
36. Nandi, K., Mazumdar, C.: Quantum teleportation of a two qubit state using GHZ-like state. Int. J. Theor. Phys. 53(4), 1322–1324 (2014). https://doi.org/10.1007/s10773-013-1928-1
37. Tang, S.Q., Shan, C.J., Zhang, X.X.: Quantum teleportation of an unknown two-atom entangled state using four-atom cluster state. Int. J. Theor. Phys. 49(8), 1899–1903 (2010). https://doi.org/10.1007/s10773-010-0373-7
38. Nie, Y.Y., et al.: Perfect teleportation of an arbitrary three-qubit state by using W-class states. Int. J. Theor. Phys. 50(10), 3225–3229 (2011). https://doi.org/10.1007/s10773-011-0825-8
39. Muralidharan, S., Panigrahi, P.K.: Perfect teleportation, quantum-state sharing, and superdense coding through a genuinely entangled five-qubit state. Phys. Rev. A. 77(3), 032321 (2008). https://doi.org/10.1103/physreva.77.032321
40. Agrawal, P., Pati, A.: Perfect teleportation and superdense coding with W states. Phys. Rev. A. 74(6), 062320 (2006). https://doi.org/10.1103/physreva.74.062320
41. Ursin, R., et al.: Quantum teleportation across the danube. Nature. 430(7002), 849 (2004). https://doi.org/10.1038/430849a
42. Joo, J., et al.: Quantum teleportation via a W state. New J. Phys. 5, 136 (2003). https://doi.org/10.1088/1367-2630/5/1/136
43. Ghosh, S., et al.: Entanglement teleportation through GHZ-class states. New J. Phys. 4, 48 (2002). https://doi.org/10.1088/1367-2630/4/1/348
44. Tsai, C.W., Hwang, T.: Teleportation of a pure EPR state via GHZ-like state. Int. J. Theor. Phys. 49(8), 1969–1975 (2010). https://doi.org/10.1007/s10773-010-0382-6
45. Da-Chuang, L., Zhuo-Liang, C.: Teleportation of two-particle entangled state via cluster state. Commun. Theor. Phys. 47(3), 464–466 (2007). https://doi.org/10.1088/0253-6102/47/3/017
46. Liu, Z.M., Zhou, L.: Quantum teleportation of a three-qubit state using a five-qubit cluster state. Int. J. Theor. Phys. 53(12), 4079–4082 (2014). https://doi.org/10.1007/s10773-014-2158-x
47. Rajiuddin, S.K., et al.: Experimental realization of quantum teleportation of an arbitrary two-qubit state using a four-qubit cluster state. Quantum Inf. Process. 19(3), 1–13 (2020). https://doi.org/10.1007/s11128-020-2586-x
48. Kumar, A., et al.: Experimental realization of controlled quantum teleportation of arbitrary qubit states via cluster states. Sci. Rep. 10(1), 13608 (2020). https://doi.org/10.1038/s41598-020-70446-8
49. Carneiro, I., et al.: Entanglement in coined quantum walks on regular graphs. New J. Phys. 7, 156 (2005). https://doi.org/10.1088/1367-2630/7/1/156
50. Wang, Y., Shang, Y., Xue, P.: Generalized teleportation by quantum walks. Quantum Inf. Process. 16(9), 1–13 (2017). https://doi.org/10.1007/s11128-017-1675-y
51. Chatterjee, Y., et al.: Experimental realization of quantum teleportation using coined quantum walks. Quantum Inf. Process. 19, 1–14 (2020). https://doi.org/10.1007/s11128-019-2527-8
52. Oh, S., Lee, S., Lee, H.W.: Fidelity of quantum teleportation through noisy channels. Phys. Rev. A. 66(2), 022316 (2002). https://doi.org/10.1103/physreva.66.022316
53. Knoll, L.T., Schmiegelow, C.T., Larotonda, M.A.: Noisy quantum teleportation: an experimental study on the influence of local environments. Phys. Rev. A. 90(4), 042332 (2014). https://doi.org/10.1103/physreva.90.042332
54. Fonseca, A.: High-dimensional quantum teleportation under noisy environments. Phys. Rev. A. 100(6), 062311 (2019). https://doi.org/10.1103/physreva.100.062311
55. Soeken, M., et al.: Window optimization of reversible and quantum circuits. In: IEEE Symposium on Design and Diagnostics of Electronic Circuits and Systems, pp. 341–345 (2010)
56. Brown, I.D., et al.: Searching for highly entangled multi-qubit states. J. Phys. A: Math. Gen. 38(5), 1119–1131 (2005). https://doi.org/10.1088/0305-4470/38/5/013
57. Anagha, M., et al.: A new scheme of quantum teleportation using highly entangled brown et al. state: an IBM quantum experience. Quantum Inf. Process. 19(5), 1–12 (2020). https://doi.org/10.1007/s11128-020-02635-3
58. Borras, A., et al.: Multiqubit systems: highly entangled states and entanglement distribution. J. Phys. A: Math. Theor. 40(44), 13407–13421 (2007). https://doi.org/10.1088/1751-8113/40/44/018
59. Choudhury, S., Muralidharan, S., Panigrahi, P.K.: Quantum teleportation and state sharing using a genuinely entangled six-qubit state. J. Phys. A: Math. Theor. 42(11), 115303 (2009). https://doi.org/10.1088/1751-8113/42/11/115303
60. Liang, Y.C., et al.: Quantum fidelity measures for mixed states. Rep. Prog. Phys. 82(7), 076001 (2019). https://doi.org/10.1088/1361-6633/ab1ca4
61. Fortes, R., Rigolin, G.: Fighting noise with noise in realistic quantum teleportation. Phys. Rev. A. 92(1), 012338 (2015). https://doi.org/10.1103/physreva.92.012338

How to cite this article: Singh, D., Kumar, S., Behera, B.K.: Complexity analysis of quantum teleportation via different entangled channels in the presence of noise. IET Quant. Comm. 4(1), 1–16 (2023). https://doi.org/10.1049/qtc2.12048

APPENDIX

The large set of density matrices equations are given in appendix.

The affected density matrices influenced by the bit-flip noise are given by the following equations from Equations (A1) to (A6). Here $|\Psi_6\rangle$ is the Borras et al. state given in Equation (9)

$$\mathcal{E}_1^B(\rho) = \frac{1}{2}\left\{\left[(1-\eta_B)^2 + (\eta_B)^2\right][|00\rangle + |11\rangle][\langle 00| + \langle 11|]\right\} \tag{A1}$$

$$\mathcal{E}_2^B(\rho) = \frac{1}{2}\left\{\left[(1-\eta_B)^3 + (\eta_B)^3\right][|000\rangle + |111\rangle][\langle 000| + \langle 111|]\right\} \tag{A2}$$

$$\begin{aligned}\mathcal{E}_3^B(\rho) = \frac{1}{4}\Big\{&\left[(1-\eta_B)^2\right][|00\rangle + |01\rangle + |10\rangle - |11\rangle][\langle 00| + \langle 01| + \langle 10| - \langle 11|] + (\eta_B)^2[|11\rangle + |01\rangle + |10\rangle - |00\rangle]\\ &[\langle 11| + \langle 01| + \langle 10| - \langle 00|]\Big\}\end{aligned} \tag{A3}$$

$$\begin{aligned}\mathcal{E}_4^B(\rho) = \frac{1}{8}\Big\{&\left[(1-\eta_B)^3\right][|000\rangle + |001\rangle + |010\rangle - |011\rangle + |100\rangle + |101\rangle - |110\rangle + |111\rangle][\langle 000| + \langle 001| + \langle 010|\\ &- \langle 011| + \langle 100| + \langle 101| - \langle 110| + \langle 111|] + (\eta_B)^3[|111\rangle + |110\rangle + |101\rangle - |100\rangle + |011\rangle + |010\rangle - |001\rangle\\ &+ |000\rangle][\langle 111| + \langle 110| + \langle 101| - \langle 100| + \langle 011| + \langle 010| - \langle 001| + \langle 000|]\Big\}\end{aligned} \tag{A4}$$

$$\begin{aligned}\mathcal{E}_5^B(\rho) = \frac{1}{8}\Big\{&\left[(1-\eta_B)^5\right][-|00101\rangle + |00111\rangle + |01000\rangle - |01010\rangle + |10001\rangle + |10011\rangle + |11100\rangle + |11110\rangle]\\ &\times[-\langle 00101| + + \langle 00111| + \langle 01000| - \langle 01010| + \langle 10001| + \langle 10011| + \langle 11100| + \langle 11110|] + (\eta_B)^5[-|11010\rangle\\ &+ |11000\rangle + |101111\rangle - |10101\rangle + |01110\rangle + |01100\rangle + |00011\rangle + |00001\rangle][-\langle 11010| + + \langle 11000| + \langle 101111|\\ &- [\langle 10101| + \langle 01110| + \langle 01100| + \langle 00011| + \langle 00001|]\Big\}\end{aligned} \tag{A5}$$

$$\mathcal{E}_6^B(\rho) = \frac{1}{32}\left\{\left[(1-\eta_B)^6\right][|\Psi_6\rangle][\langle\Psi_6|] + (\eta_B)^6\left[|\chi_6^B\rangle\langle\chi_6^B|\right]\right\} \tag{A6}$$

where $|\chi_6^B\rangle$ is given by

$$\begin{aligned}|\chi_6^B\rangle = [&|111111\rangle + |000000\rangle + |111100\rangle + |000011\rangle + |111010\rangle + |000101\rangle + |111001\rangle + |000110\rangle + |110110\rangle + |001001\rangle\\ &+ |110000\rangle + |001111\rangle + |101110\rangle + |010001\rangle + |101010\rangle + |010010\rangle + |100111\rangle + |011000\rangle + |100010\rangle + |011101\rangle\\ &- |110101\rangle - |001010\rangle - |110011\rangle - |001100\rangle - |101011\rangle - |010100\rangle - |101000\rangle - |010111\rangle - |100100\rangle - |011011\rangle\\ &- |100001\rangle - |011110\rangle]\end{aligned} \tag{A7}$$

The affected density matrices influenced by the phase-flip noise are given by the following equations from Equations (A8) to (A13). Here $|\Psi_6\rangle$ is the Borras et al. state given in Equation (9).

$$\mathcal{E}_1^W(\rho) = \frac{1}{2}\left\{\left[(1-\eta_W)^2 + \eta_W^2\right][|00\rangle + |11\rangle][\langle 00| + \langle 11|]\right\} \tag{A8}$$

$$\mathcal{E}_2^W(\rho) = \frac{1}{2}\left\{(1-\eta_W)^3[|000\rangle + |111\rangle][\langle 000| + \langle 111|] + (\eta_W)^3[|00\rangle - |11\rangle][\langle 00| - \langle 11|]\right\} \tag{A9}$$

$$\begin{aligned}\mathcal{E}_3^W(\rho) = \frac{1}{4}\Big\{&\left[(1-\eta_W)^2\right][|00\rangle + |01\rangle + |10\rangle - |11\rangle][\langle 00| + \langle 01| + \langle 10| - \langle 11|] + (\eta_W)^2[|00\rangle - |01\rangle - |10\rangle - |11\rangle]\\ &[\langle 00| - \langle 01| - \langle 10| - \langle 11|]\Big\}\end{aligned} \tag{A10}$$

$$\mathcal{E}_4^W(\rho)=\frac{1}{8}\Big\{\Big[\big(1-\eta_W\big)^3\Big][|000\rangle+|001\rangle+|010\rangle-|011\rangle+|100\rangle+|101\rangle-|110\rangle+|111\rangle][\langle 000|+\langle 001|+\langle 010| -\langle 011|+\langle 100|+\langle 101|-\langle 110|+\langle 111|]+\big(\eta_W\big)^3[|000\rangle-|001\rangle-|010\rangle-|011\rangle-|100\rangle+|101\rangle-|110\rangle -|111\rangle][\langle 000|-\langle 001|-\langle 010|-\langle 011|-\langle 100|+\langle 101|-\langle 110|-\langle 111|]\Big\} \tag{A11}$$

$$\mathcal{E}_5^W(\rho)=\frac{1}{2}\Big\{\Big[\big(1-\eta_W\big)^5\Big][-|00101\rangle+|00111\rangle+|01000\rangle-|01010\rangle+|10001\rangle+|10011\rangle+|11100\rangle+|11110\rangle] [-\langle 00101|+\langle 00111|+\langle 01000|-\langle 01010|+\langle 10001|+\langle 10011|+\langle 11100|+\langle 11110|]+\big(\eta_W\big)^5[-|00101\rangle -|00111\rangle-|01000\rangle-|01010\rangle+|10001\rangle-|10011\rangle-|11100\rangle+|11110\rangle][-\langle 00101|-\langle 00111| -\langle 01000|-\langle 01010|+\langle 10001|-\langle 10011|-\langle 11100|+\langle 11110|]\Big\} \tag{A12}$$

$$\mathcal{E}_6^W(\rho)=\frac{1}{32}\Big\{\big(1-\eta_W\big)^6[|\Psi_6\rangle][\langle\Psi_6|]+\big(\eta_W\big)^6\big[|\chi_6^W\rangle\langle\chi_6^W|\big]\Big\} \tag{A13}$$

where the quantum state $|\chi_6^W\rangle$ is given by Equation (A14)

$$\begin{aligned}|\chi_6^W\rangle=&|000000\rangle+|111111\rangle+|000011\rangle+|111100\rangle+|000101\rangle+|111010\rangle+|000110\rangle+|111001\rangle+|001001\rangle+|110110\rangle\\&+|001111\rangle+|110000\rangle+|010001\rangle+|101110\rangle+|010010\rangle+|101101\rangle+|011000\rangle+|100111\rangle+|011101\rangle+|100010\rangle\\&-|001010\rangle-|110101\rangle-|001100\rangle-|110011\rangle-|010100\rangle-|101011\rangle-|010111\rangle-|101000\rangle-|011011\rangle-|100100\rangle\\&-|011110\rangle-|100001\rangle\end{aligned} \tag{A14}$$

The affected density matrices influenced by the bit-phase-flip noise are given by the following equations from Equations (A15) to (A20). Here $|\Psi_6\rangle$ is the Borras et al. state given in Equation (9).

$$\mathcal{E}_1^F(\rho)=\frac{1}{2}\Big\{\big(1-\eta_F\big)^2[|00\rangle+|11\rangle][\langle 00|+\langle 11|]+\big(\eta_F\big)^2[|00\rangle-|11\rangle][\langle 00|-\langle 11|]\Big\} \tag{A15}$$

$$\mathcal{E}_2^F(\rho)=\frac{1}{2}\Big\{\big(1-\eta_F\big)^3[|000\rangle+|111\rangle][\langle 000|+\langle 111|]-\eta_F^3[|111\rangle-|000\rangle][\langle 111|-\langle 000|]\Big\} \tag{A16}$$

$$\mathcal{E}_3^F(\rho)=\frac{1}{4}\Big\{\Big[\big(1-\eta_F\big)^2\Big][|00\rangle+|01\rangle+|10\rangle-|11\rangle][\langle 00|+\langle 01|+\langle 10|-\langle 11|]+\big(\eta_F\big)^2[|11\rangle-|01\rangle-|10\rangle-|00\rangle] [\langle 11|-\langle 01|-\langle 10|-\langle 00|]\Big\} \tag{A17}$$

$$\mathcal{E}_4^F(\rho)=\frac{1}{8}\Big\{\Big[\big(1-\eta_F\big)^3\Big][|000\rangle+|001\rangle+|010\rangle-|011\rangle+|100\rangle+|101\rangle-|110\rangle+|111\rangle][\langle 000|+\langle 001|+\langle 010| -\langle 011|+\langle 100|+\langle 101|-\langle 110|+\langle 111|]+\big(i\eta_F\big)^3[|111\rangle-|110\rangle-|101\rangle-|100\rangle-|011\rangle+|010\rangle-|001\rangle -|000\rangle][\langle 111|-\langle 110|-\langle 101|-\langle 100|-\langle 011|+\langle 010|-\langle 001|-\langle 000|]\Big\} \tag{A18}$$

$$\mathcal{E}_5^F(\rho)=\frac{1}{8}\Big\{\Big[\big(1-\eta_F\big)^5\Big][-|00101\rangle+|00111\rangle+|01000\rangle-|01010\rangle+|10001\rangle+|10011\rangle+|11100\rangle+|11110\rangle] [-\langle 00101|+\langle 00111|+\langle 01000|-\langle 01010|+\langle 10001|+\langle 10011|+\langle 11100|+\langle 11110|]+i\big(\eta_F\big)^5[-|11010\rangle -|11000\rangle-|101111\rangle-|10101\rangle+|01110\rangle-|01100\rangle-|00011\rangle+|00001\rangle][-\langle 11010|-\langle 11000|-\langle 10111| -\langle 10101|+\langle 01110|-\langle 01100|-\langle 00011|+\langle 00001|]\Big\} \tag{A19}$$

$$\mathcal{E}_6^F(\rho) = \frac{1}{32}\left\{(1-\eta_F)^6[|\Psi_6\rangle][\langle\Psi_6|] + (\eta_F)^6\left[|\chi_6^B\rangle\langle\chi_6^B|\right]\right\} \tag{A20}$$

The affected density matrices influenced by the amplitude damping noise are given by the following equations from Equations (A21) to (A26)

$$\mathcal{E}^A(\rho) = \frac{1}{2}\left\{\left[|00\rangle + (1-\eta_A)|11\rangle\right]\left[\langle 00| + (1-\eta_A)\langle 11|\right] + (\eta_A)^2[|00\rangle\langle 00|]\right\} \tag{A21}$$

$$\mathcal{E}_2^A(\rho) = \frac{1}{2}\left\{\left[|000\rangle + (1-\eta_A)^{\frac{3}{2}}|111\rangle\right]\left[\langle 000| + (1-\eta_A)^{\frac{3}{2}}\langle 111|\right] + (\eta_A)^3[|000\rangle\langle 000|]\right\} \tag{A22}$$

$$\mathcal{E}_3^A(\rho) = \frac{1}{4}\left\{\left[|00\rangle + \sqrt{1-\eta_A}\,(|01\rangle + |10\rangle - |11\rangle)\right]\left[\langle 00| + \sqrt{1-\eta_A}\,(\langle 01| + \langle 10| - \langle 11|)\right] + (\eta_A)^2[|00\rangle][\langle 00|]\right\} \tag{A23}$$

$$\begin{aligned}\mathcal{E}_4^A(\rho) = \frac{1}{8}\Bigg\{&\left[|000\rangle + \sqrt{(1-\eta_A)}\;(|001\rangle + |010\rangle - |100\rangle) + (1-\eta_A)^2(|011\rangle + |101\rangle - |110\rangle) + \sqrt{(1-\eta_A)^3}\,|111\rangle\right]\\ &\left[\langle 000| + \sqrt{(1-\eta_A)}\,(\langle 001| + \langle 010| - \langle 100|) + (1-\eta_A)^2(\langle 011| + \langle 101| - \langle 110|)\right.\\ &\left.+ \sqrt{(1-\eta_A)^3}\,\langle 111|\right] + (\eta_A)^3[|000\rangle][\langle 000|]\Bigg\}\end{aligned} \tag{A24}$$

$$\begin{aligned}\mathcal{E}_5^A(\rho) = \frac{1}{8}\Bigg\{&\left[\sqrt{1-\eta_A}\,|01000\rangle + (1-\eta_A)(-|00101\rangle + |10001\rangle - |01010\rangle) + \sqrt{(1-\eta_A)^3}\,(|00111\rangle + |10011\rangle\right.\\ &\left.+ |11100\rangle) + (1-\eta_A)^2|11110\rangle\right]\left[\sqrt{1-\eta_A}\langle 01000| + (1-\eta_A)(-\langle 00101| + \langle 10001| - \langle 01010|)\right.\\ &\left.+ \sqrt{(1-\eta_A)^3}\,(\langle 00111| + \langle 10011| + \langle 11100|) + (1-\eta_A)^2\langle 11110|\right]\Bigg\}\end{aligned} \tag{A25}$$

$$\begin{aligned}\mathcal{E}_6^A(\rho) = \frac{1}{32}\Big\{&[|000000\rangle + (1-\eta_A)^3|111111\rangle + (1-\eta_A)(|000011\rangle + |000101\rangle + |000110\rangle + |001001\rangle + |010001\rangle\\ &+ |110000\rangle + |010010\rangle + |011000\rangle + |100010\rangle - |001010\rangle - |001100\rangle - |010100\rangle - |101000\rangle - |100100\rangle\\ &- |100001\rangle) + (1-\eta_A)^2(|111100\rangle + |111010\rangle + |111001\rangle + |110110\rangle + |001111\rangle + |101110\rangle + |101101\rangle\\ &+ |100111\rangle + |011101\rangle + |110101\rangle - |110011\rangle - |101011\rangle + +|010111\rangle - |011011\rangle - |011110\rangle)][\langle 000000|\\ &+ (1-\eta_A)^3\langle 111111| + (1-\eta_A)(\langle 000011| + \langle 000101| + \langle 000110| + \langle 001001| + \langle 010001| + \langle 110000|\\ &+ \langle 010010| + \langle 011000| + \langle 100010| - \langle 001010| - \langle 001100| - \langle 010100| - \langle 101000| - \langle 100100| - \langle 100001|)\\ &+ (1-\eta_A)^2(\langle 111100| + \langle 111010| + \langle 111001| + \langle 110110| + \langle 001111| + \langle 101110| + \langle 101101| + \langle 100111|\\ &+ \langle 011101| + \langle 110101| - \langle 110011| - \langle 101011| + \langle 010111| - \langle 011011| - \langle 011110|)] + (\eta_A)^6[|000000\rangle][\langle 000000|]\Big\}\end{aligned} \tag{A26}$$

The affected density matrices influenced by the phase damping noise are given by the following equations from Equations (A27) to (A32)

$$\mathcal{E}_1^P(\rho) = \frac{1}{2}\left\{(1-\eta_P)^2[|00\rangle + |11\rangle][\langle 00| + \langle 11|] + (\eta_P)^2[|00\rangle\langle 00| + |11\rangle\langle 11|]\right\} \tag{A27}$$

$$\mathcal{E}_2^P(\rho) = \frac{1}{2}\left\{(1-\eta_P)^3[|000\rangle + |111\rangle][\langle 000| + \langle 111|] + (\eta_P)^3[|000\rangle\langle 000| + |111\rangle\langle 111|]\right\} \tag{A28}$$

$$\mathcal{E}_3^P(\rho)=\frac{1}{4}\Big\{(1-\eta_P)^2[|00\rangle+|01\rangle+|10\rangle-|11\rangle][\langle 00|+\langle 01|+\langle 10|-\langle 11|]+(\eta_P)^4[|00\rangle\langle 00|][|11\rangle\langle 11|]\Big\} \tag{A29}$$

$$\begin{aligned}\mathcal{E}_4^P(\rho)=\frac{1}{8}\Big\{\Big[(1-\eta_P)^3\Big][|000\rangle+|001\rangle+|010\rangle-|011\rangle+|100\rangle+|101\rangle-|110\rangle+|111\rangle][\langle 000|+\langle 001|+\langle 010|\\ -\langle 011|+\langle 100|+\langle 101|-\langle 110|+\langle 111|]+(\eta_P)^3[|000\rangle\langle 000|+|111\rangle\langle 111|]\Big\}\end{aligned} \tag{A30}$$

$$\begin{aligned}\mathcal{E}_5^P(\rho)=\frac{1}{8}\Big\{(1-\eta_A)^5[-|00101\rangle+|00111\rangle+|01000\rangle-|01010\rangle+|10001\rangle+|10011\rangle+|11100\rangle+|11110\rangle]\\ [-\langle 00101|+\langle 00111|+\langle 01000|-\langle 01010|+\langle 10001|+\langle 10011|+\langle 11100|+\langle 11110|]\}\end{aligned} \tag{A31}$$

$$\mathcal{E}_6^P(\rho)=\frac{1}{32}\Big\{(1-\eta_P)^6[|\Psi_6\rangle\langle\Psi_6|]+(\eta_P)^6[|000000\rangle\langle 000000|+|111111\rangle\langle 111111|]\Big\} \tag{A32}$$

The affected density matrices influenced by the depolarising noise are given by the following equations from Equations (A33) to (A38). Here $|\Psi_3\rangle$, $|\Psi_5\rangle$ and $|\Psi_6\rangle$ are the three-qubit cluster state, Brown et al. and Borras et al. state given in Equations (5), (9) and (7) respectively.

$$\mathcal{E}_1^D(\rho)=\frac{1}{2}\Big\{\Big[(1-\eta_D)^2+\frac{\eta_D^2}{3}\Big][|00\rangle+|11\rangle][\langle 00|+\langle 11|]\Big\} \tag{A33}$$

$$\mathcal{E}_2^D(\rho)=\frac{1}{2}\Big\{\Big[(1-\eta_D)^3+\frac{{\eta_D}^3}{27}+i\frac{{\eta_D}^3}{27}\Big][|000\rangle+|111\rangle][\langle 000|+\langle 111|]+\Big(\frac{\eta_D^3}{27}\Big)[|000\rangle-|111\rangle][\langle 000|-\langle 111|]\Big\} \tag{A34}$$

$$\begin{aligned}\mathcal{E}_3^D(\rho)=\frac{1}{4}\Big\{(1-\eta_D)^2[|00\rangle+|01\rangle+|10\rangle-|11\rangle][\langle 00|+\langle 01|+\langle 10|-\langle 11|]+2\frac{\eta_D^2}{9}[|11\rangle+|10\rangle+|01\rangle-|00\rangle]\\ \big[\langle 11|+\langle 10|+\langle 01|-\langle 00|]+\frac{\eta_D^2}{9}[|00\rangle-|01\rangle-|10\rangle-|11\rangle][\langle 00|-\langle 01|-\langle 10|-\langle 11|]\Big\}\end{aligned} \tag{A35}$$

$$\begin{aligned}\mathcal{E}_4^D(\rho)=\frac{1}{8}\Big\{\Big[(1-\eta_D)^3\Big][|\Psi_4\rangle][\langle\Psi_4|]+\Big(\frac{\eta_D}{3}\Big)^3[|111\rangle+|110\rangle+|101\rangle-|100\rangle+|011\rangle+|010\rangle-|001\rangle+|000\rangle][\langle 111|+\langle 110|\\ +\langle 101|-\langle 100|+\langle 011|+\langle 010|-\langle 001|+\langle 000|]-\Big(\frac{\eta_D}{3}\Big)^3[|111\rangle-|110\rangle-|101\rangle-|100\rangle-|011\rangle\\ +|010\rangle-|001\rangle-|000\rangle][\langle 111|-\langle 110|-\langle 101|-\langle 100|-\langle 011|+\langle 010|-\langle 001|-\langle 000|]+\Big(\frac{\eta_D}{3}\Big)^3[|000\rangle\\ -|001\rangle-|010\rangle-|011\rangle-|100\rangle+\ |101\rangle-|110\rangle-|111\rangle][\langle 000|-\langle 001|-\langle 010|-\langle 011|-\langle 100|+\langle 101|\\ -\langle 110|-\langle 111|\Big\}\end{aligned} \tag{A36}$$

$$\begin{aligned}\mathcal{E}_5^D(\rho)=\frac{1}{8}\Big\{\Big[(1-\eta_D)^5\Big][|\Psi_5\rangle][\langle\Psi_5|]+\Big(\frac{\eta_D}{3}\Big)^5[-|11010\rangle+|11000\rangle+|101111\rangle-|10101\rangle+|01110\rangle+|01100\rangle+|00011\rangle\\ +|00001\rangle][-\langle 11010|+\langle 11000|+\langle 101111|-\langle 10101|+\langle 01110|+\langle 01100|+\langle 00011|+\langle 00001|]+\Big(\frac{\eta_D}{3}\Big)^5[-|00101\rangle\\ -|00111\rangle-|01000\rangle-|01010\rangle+|10001\rangle-|10011\rangle-|11100\rangle+|11110\rangle][-\langle 00101|-\langle 00111|-\langle 01000|-\langle 01010|\\ +\langle 10001|-\langle 10011|-\langle 11100|+\langle 11110|]-\Big(\frac{\eta_D}{3}\Big)^5[-|11010\rangle-|11000\rangle-|101111\rangle-|10101\rangle+|01110\rangle-|01100\rangle\\ -|00011\rangle+|00001\rangle][-\langle 11010|-\langle 11000|-\langle 10111|-\langle 10101|+\langle 01110|-\langle 01100|-\langle 00011|+\langle 00001|]\Big\}\end{aligned} \tag{A37}$$

$$\mathcal{E}_6^D(\rho)=\frac{1}{32}\Big\{[|\Psi_6\rangle][\langle\Psi_6|]+2\Big(\frac{\eta_D}{3}\Big)^6[|\chi_6^B\rangle\langle\chi_6^B|]+\Big(\frac{\eta_D}{3}\Big)^6[|\chi_6^W\rangle\langle\chi_6^W|]\Big\} \tag{A38}$$

where $|\chi_6^B\rangle$ and $|\chi_6^W\rangle$ are the quantum states given in Equations (A7) and (A14) respectively.